Acta Crystallographica Section B
Structural Science
ISSN 0108-7681

Hypothetical binodal zeolitic frameworks

Alexandra Simperler,[a] Martin D. Foster,[a] Olaf Delgado Friedrichs,[b] Robert G. Bell,[a] Filipe A. Almeida Paz[c,d] and Jacek Klinowski[c]*

[a]Davy–Faraday Research Laboratory, The Royal Institution of Great Britain, 21 Albemarle Street, London W1S 4BS, England, [b]Department of Chemistry and Biochemistry, Arizona State University, Tempe, AZ 85287-1604, USA, [c]Department of Chemistry, University of Cambridge, Lensfield Road, Cambridge CB2 1EW, England, and [d]Department of Chemistry, CICECO, University of Aveiro, Campus Universitário de Santiago, Aveiro 3810-193, Portugal

Correspondence e-mail: jk18@cam.ac.uk

Received 19 April 2005
Accepted 27 April 2005

Hypothetical binodal zeolitic structures (structures containing two kinds of tetrahedral sites) were systematically enumerated using tiling theory and characterized by computational chemistry methods. Each of the 109 refineable topologies based on 'simple tilings' was converted into a silica polymorph and its energy minimized using the *GULP* program with the Sanders–Catlow silica potential. Optimized structural parameters, framework energies relative to α-quartz and volumes accessible to sorption have been calculated. Eleven of the 30 known binodal topologies listed in the Atlas of Zeolite Framework Types were found, leaving 98 topologies that were unknown previously. The chemical feasibility of each structure as a zeolite was evaluated by means of a feasibility factor derived from the correlation between lattice energy and framework density. Structures are divided into 15 families, based on common structural features. Many 'feasible' structures contain only small pores. Several very open structures were also enumerated, although they contain three-membered rings which are thermodynamically disfavoured and not found in conventional zeolites. We believe that such topologies may be realizable as framework materials, but with different elemental compositions to those normally associated with zeolites.

1. Introduction

Zeolites find many important applications in science and technology in areas as diverse as catalysis, chemical separation, water softening, agriculture, refrigeration and optoelectronics. There are 152 distinct structural types of zeolites which have now been identified (Baerlocher *et al.*, 2001). The definition of a zeolite is based not on chemical composition or function, but rather on atomic scale geometry. In order to qualify as a zeolite or zeolite-type material (zeotype), a mineral or synthetic material must possess a framework composed of corner-sharing tetrahedra. There is an additional requirement of 'openness', simultaneously dependent on density and smallest ring size, thus excluding denser minerals. Another way of expressing this is in terms of a four-connected net in which each vertex (in chemical terms the central atom of a tetrahedron) is connected to its four closest neighbours, normally *via* an oxygen bridge.

The enumeration of hypothetical zeolitic framework structures (Klinowski, 1998) is of considerable scientific and practical interest in terms of generating new nanoporous architectures. Enumeration originates with the work of Wells (1977, 1979, 1984) on three-dimensional nets and polyhedra. Smith and collaborators (Smith, 1988, 1993; Alberti, 1979; Sato, 1984, 1987; Sherman & Bennett, 1973; Barrer & Villiger, 1969), O'Keeffe and collaborators (O'Keeffe & Hyde,

1996*a*,*b*) and Akporiaye & Price (1989) found many possible new structures by combining various structural subunits. More recent work involves computer search algorithms (Boisen *et al.*, 1999; Treacy *et al.*, 1997; Foster & Treacy, 2004; Mellot-Draznieks *et al.*, 2000).

Our work is based on advances in combinatorial tiling theory (Dress *et al.*, 1993). A tiling is a periodic subdivision of three-dimensional space into connected regions, which we call *tiles*. If two tiles meet along a surface, the surface is called a *face*. If three or more faces meet along a curve, we call the curve an *edge*. If at least three edges meet at a point, we call that point a *vertex*. A network is thus formed by the vertices and edges. The configuration of edges, faces and tiles around a given vertex can be described *via* the so-called vertex figure, obtained by placing the centre of a small notational sphere at the vertex and considering the tiling of that sphere formed by the intersections with the different tiles touching that vertex. We have already enumerated all possible Euclidean uni-, bi- and trinodal tilings based on simple vertex figures and all uninodal tilings with vertex figures containing up to six extra edges (Delgado Friedrichs, 2001), and the computer program used for this task is available from the authors upon request (`olaf.delgado@asu.edu`).

The tiling approach identified networks with one, two and three types of inequivalent vertices, which we call uninodal, binodal and trinodal (Delgado Friedrichs *et al.*, 1999). We have shown that there are exactly 9, 117 and over 1300 topological types of four-connected uninodal, binodal and trinodal nets, respectively, which are based on 'simple' periodic tilings (as explained in Delgado Friedrichs *et al.*, 1999). The previously reported number of 926 for the trinodal simple tilings included, due to an error in the manual processing of the data files, only those nets for which the tiles have non-trivial site symmetry. In addition, there are at least 157 additional uninodal nets derived from 'quasi-simple' tilings (the vertex figures of which are derived from tetrahedra, but contain double edges; Delgado Friedrichs *et al.*, 1999) and which have already been discussed elsewhere (Foster *et al.*, 2001, 2003; Foster, Friedrichs *et al.*, 2004; Foster, Simperler *et al.*, 2004; Simperler *et al.*, 2004;). For example, zeolitic structure types SOD, LTA,

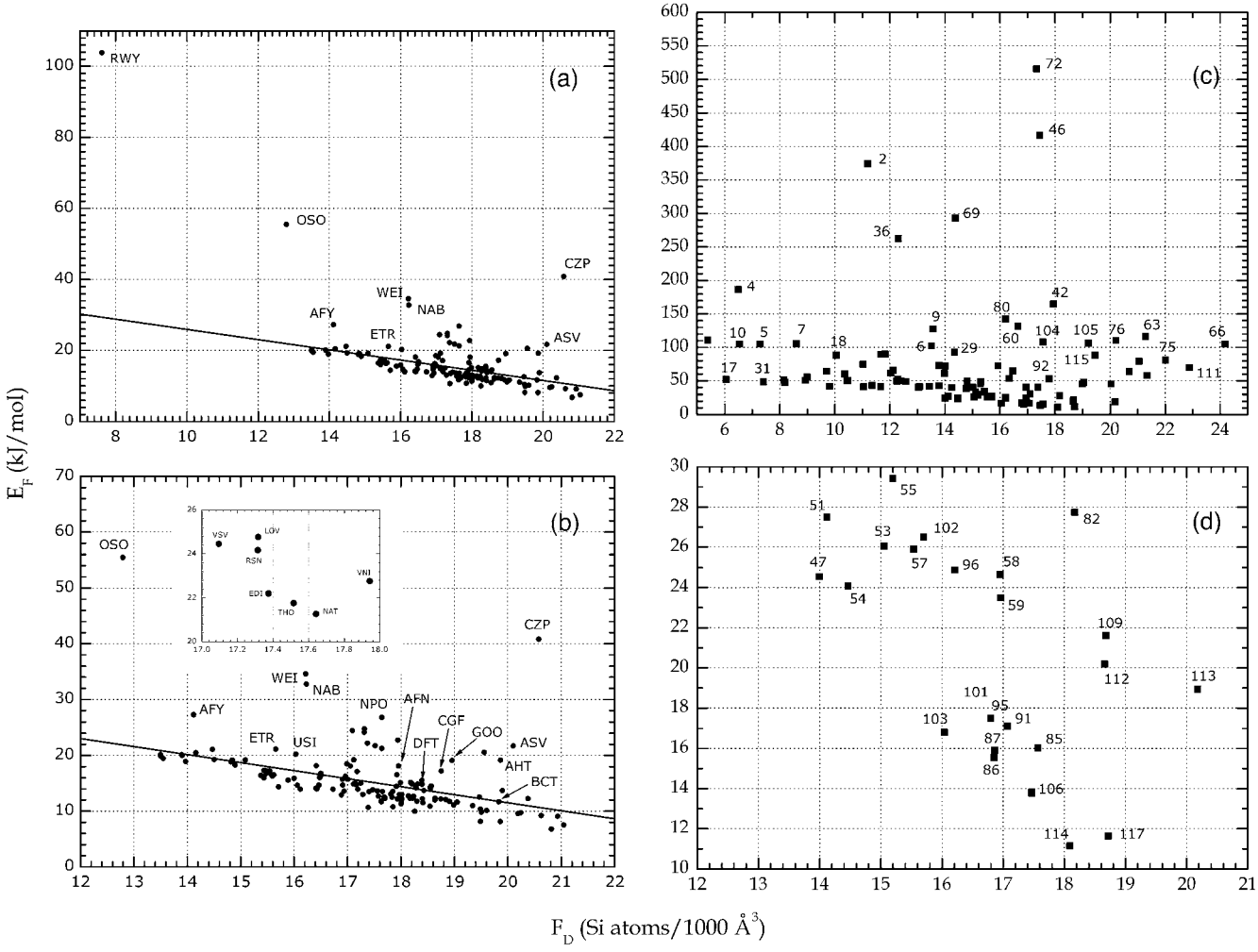

Figure 1
Framework energy, E_F (kJ mol^{-1}), with respect to α-quartz, *versus* framework density, F_D (Si atoms per 1000 Å^3), for (*a*) and (*b*) all known zeolitic structure types; (*c*) and (*d*) hypothetical binodal zeolitic structures.

Table 1
Chemical feasibility factor, relative lattice energy, framework density and coordination sequences for 109 hypothetical binodal zeolites, optimized as purely siliceous structures.

Structures are listed in order of increasing value of ϑ.

Structure	ϑ	ΔE_{quartz} (kJ mol^{-1})	F_D (T sites per 1000 Å^3)	Coordination sequence									
2_87	0.10	15.91	16.86	4	9	17	30	49	72	96	121	150	187
				4	10	20	33	49	69	94	125	160	197
2_89 (ERI)	0.12	16.39	16.51	4	9	17	30	50	75	98	118	144	185
				4	10	20	32	46	64	90	126	164	196
2_84 (EAB)	0.12	16.41	16.49	4	9	17	30	49	71	92	115	147	190
				4	10	20	32	46	66	94	128	162	192
2_90 (SAT)	0.18	15.72	16.91	4	9	17	30	50	75	100	126	157	194
				4	10	20	33	50	71	95	124	158	197
2_103	0.30	16.80	16.04	4	10	17	30	52	70	107	128	166	208
				4	11	20	33	51	73	103	136	169	207
2_88 (AWW)	0.32	15.03	17.25	4	9	17	30	50	74	97	123	158	198
				4	10	20	33	50	72	98	128	162	200
2_86	0.37	15.54	16.85	4	9	17	30	49	72	96	121	150	186
				4	10	20	33	49	68	92	122	155	191
2_83 (LEV)	0.42	16.00	16.48	4	9	17	30	49	71	92	114	143	183
				4	10	20	32	46	64	90	124	156	184
2_85	0.69	16.03	17.57	4	9	17	30	49	71	95	125	161	201
				4	10	20	33	50	73	100	131	168	208
2_107 (LOS)	0.91	13.86	17.47	4	10	20	34	52	74	102	136	172	210
				4	10	20	34	54	78	104	134	168	210
2_74 (TSC)	0.94	19.47	13.55	4	9	16	25	37	53	74	99	125	151
				4	9	17	28	41	56	73	93	117	146
2_110	0.94	13.82	17.47	4	9	17	30	50	74	97	123	158	198
				4	10	20	33	50	72	98	128	162	200
2_106	0.97	13.79	17.46	4	10	20	34	52	74	100	130	166	208
				4	10	20	34	53	76	103	135	170	209
2_95	0.93	17.49	16.80	4	9	18	32	52	75	99	133	171	207
				4	10	19	32	52	76	103	136	172	213
2_108	0.97	13.77	17.47	4	10	20	34	53	76	102	132	167	208
				4	10	20	34	53	76	103	135	170	208
2_81 (SAS)	0.98	15.88	16.00	4	9	17	30	48	68	87	109	142	184
				4	10	19	30	45	65	90	118	145	175
2_91	0.95	17.12	17.07	4	9	17	31	54	82	108	137	176	223
				4	11	22	35	55	81	107	143	184	222
2_78 (AFX)	1.00	16.41	15.61	4	9	17	29	45	64	85	110	141	178
				4	9	17	29	45	65	89	116	144	175
2_101 (AST)	0.99	18.14	16.41	4	9	19	34	48	66	96	127	151	183
				4	12	18	28	52	78	88	112	162	204
2_117	1.22	11.58	18.74	4	11	24	41	64	93	127	163	205	255
				4	12	22	44	64	94	124	164	206	252
2_114	2.17	11.15	18.09	4	11	21	36	64	93	120	156	202	255
				4	11	23	40	62	88	123	162	202	249
2_47	3.02	24.55	14.00	4	9	17	28	41	56	74	97	125	158
				4	8	14	24	37	54	75	97	121	148
2_54	3.18	24.09	14.47	4	8	14	25	40	57	76	96	119	150
				4	9	17	27	38	54	76	101	128	154
2_112	4.66	20.19	18.66	4	10	22	40	60	95	121	165	212	258
				4	12	21	41	67	90	128	168	211	263
2_50 (AFY)	5.03	27.27	14.12	4	8	14	25	39	53	71	96	124	152
				4	9	16	23	34	57	82	98	115	141
2_53	5.11	26.05	15.05	4	7	12	24	39	60	79	110	168	250
				4	10	19	27	39	62	92	137	202	275
2_51	5.18	27.49	14.12	4	8	14	25	39	53	72	100	130	157
				4	9	16	23	34	57	82	98	118	153
2_59	5.25	23.49	16.96	4	9	18	32	52	75	99	133	171	207
				4	10	19	32	52	76	103	136	172	213
2_113	5.32	18.94	20.19	4	10	23	38	60	86	118	154	195	244
				4	11	21	39	61	86	118	154	195	243
2_96	5.45	24.88	16.21	4	9	18	32	52	75	105	144	181	217
				4	11	21	35	54	80	113	145	182	228
2_57	5.51	25.91	15.54	4	8	14	26	44	63	80	97	122	164
				4	10	19	28	39	57	82	112	139	159
2_109	5.67	21.61	18.68	4	10	20	34	53	76	102	133	170	212
				4	10	20	34	53	77	106	139	174	212
2_58	6.04	24.64	16.95	4	8	14	26	45	67	89	115	149	188
				4	10	20	32	47	68	93	122	157	196

RHO, FAU, KFI and CHA are all based on quasi-simple tilings. An example of a non-simple tiling is that of GIS, where the tile has some two-connected vertices.

Here we focus our attention on the binodal structures, *i.e.* those with two topologically inequivalent types of tetrahedral vertex (T-atom sites) derived only from simple tilings, meaning that they can be readily described by the packing of convex polyhedra, the vertices of which are all three-connected. Structures containing cages are thus found in abundance, while those with, for instance, more 'cylindrical' channels are less common and tend to have lower framework density than the 'quasi-simple' structures, with a greater proportion lying in the range of density where most known zeolites are found, as opposed to denser minerals. On the other hand, many of the known zeolite structure types cannot be constructed from simple tilings. Thus, simple tilings cannot generate the complete set of binodal zeolites. Seven of the 21 known *uninodal* zeolites correspond to simple tilings, and the remaining 14, together with several mineral structures (although not quartz) are constructed using quasi-simple tilings. We have found 11 of the 30 known binodal zeolite types, and the remaining 19 will be found by considering quasi-simple tilings, just as with the uninodal structures. The number of potential binodal networks thus generated will be enormous, and their enumeration will require the use of state-of-the-art computational facilities. However, only very few binodal structures have previously been enumerated, while nearly all uninodal structures derived from the tilings were previously known, either as crystal structures or as hypothetical nets. It is therefore of interest to describe the binodal structures derived only from simple tilings.

To characterize the structures, we follow procedures identical to

Table 1 (continued)

Structure	ϑ	ΔE_{quartz} (kJ mol^{-1})	F_D (T sites per 1000 Å^3)	Coordination sequence									
2_102	6.08	26.50	15.70	4	9	19	34	48	73	98	125	167	197
				4	11	18	31	54	72	96	128	160	204
2_55	7.61	29.43	15.20	4	8	14	26	44	62	91	121	144	181
				4	11	19	29	47	67	91	121	153	188
2_82	9.41	27.74	18.17	4	9	17	30	48	69	92	119	153	192
				4	10	20	32	46	66	94	126	158	194
2_67	10.27	33.41	15.11	4	8	16	28	42	60	84	108	136	170
				4	9	16	27	43	62	83	109	139	171
2_99	10.53	30.91	17.10	4	9	18	34	55	76	103	144	187	229
				4	9	20	34	54	81	110	144	185	229
2_35	10.69	41.65	9.82	4	8	13	20	28	36	46	62	83	104
				4	9	15	21	28	37	49	65	85	108
2_62	10.97	33.96	15.43	4	8	14	27	48	70	91	116	146	185
				4	9	19	32	45	67	92	124	165	209
2_43	11.62	41.22	11.05	4	8	14	21	34	53	71	90	108	133
				4	8	16	27	35	48	66	83	113	146
2_64	12.15	41.09	11.67	4	8	15	25	37	52	71	95	120	148
				4	8	16	27	37	53	71	89	116	144
2_45	12.91	40.22	13.03	4	8	14	23	34	49	67	87	111	139
				4	9	16	25	37	52	70	91	114	140
2_31	13.16	48.71	7.40	4	8	12	17	24	31	36	42	54	72
				4	9	15	20	24	29	37	48	60	73
2_24	13.28	43.16	11.36	4	7	12	22	32	41	56	80	106	125
				4	9	15	22	32	46	63	81	100	122
2_19	13.39	47.93	8.17	4	7	10	16	22	26	34	48	63	76
				4	8	12	16	21	28	37	49	64	80
2_73	13.62	38.71	14.78	4	9	15	21	37	59	104	138	182	199
				4	11	20	36	52	77	121	155	192	236
2_68	13.82	41.46	13.08	4	8	17	28	45	66	88	114	141	182
				4	9	16	28	48	66	84	115	150	178
2_39	13.86	39.83	14.25	4	8	13	22	36	53	72	94	122	156
				4	9	16	25	38	56	78	103	129	157
2_17	13.96	51.80	6.05	4	7	9	13	19	23	25	30	41	55
				4	8	12	15	17	21	28	36	44	53
2_70	14.33	41.70	13.42	4	8	17	32	46	71	95	129	166	199
				4	9	18	32	50	70	95	128	166	212
2_40	14.97	40.32	15.02	4	8	13	22	37	56	76	98	126	158
				4	9	16	26	41	60	80	101	126	158
2_27	15.42	42.76	13.78	4	7	12	24	38	50	68	94	122	153
				4	9	16	26	40	57	78	103	130	159
2_23	15.97	51.69	8.14	4	7	12	20	26	32	44	68	90	108
				4	8	13	17	24	34	49	67	82	101
2_20	16.11	50.76	8.93	4	7	10	17	27	35	41	52	73	100
				4	9	15	20	25	33	47	66	84	98
2_97	16.99	40.46	16.94	4	9	18	32	52	76	106	147	188	229
				4	11	21	35	55	81	117	152	188	238
2_71	17.07	39.95	17.38	4	8	19	39	58	83	118	160	193	232
				4	10	21	38	58	91	117	158	195	244
2_26	17.51	50.60	10.44	4	7	12	22	34	46	58	76	107	139
				4	8	14	21	32	48	65	86	111	138
2_25	17.56	50.63	10.47	4	7	12	22	33	44	58	80	104	125
				4	8	14	21	32	48	65	85	106	132
2_37	18.50	48.93	12.58	4	8	12	17	24	31	36	42	54	72
				4	9	15	20	24	29	37	48	60	73
2_21	18.85	49.90	12.26	4	7	10	18	32	47	59	71	91	121
				4	9	16	24	34	48	66	89	117	149
2_32	19.04	49.98	12.40	4	8	12	18	29	44	60	77	98	125
				4	9	16	24	33	45	62	85	113	143
2_48	19.09	45.87	15.29	4	8	14	25	38	50	70	100	125	147
				4	9	16	24	36	56	76	92	120	159
2_41	19.44	55.48	8.99	4	8	14	19	26	40	52	70	88	100
				4	8	14	20	29	42	52	68	89	109
2_69	20.57	49.50	14.25	4	8	17	29	46	68	91	117	154	184
				4	9	17	28	49	69	92	119	151	184
2_65	20.64	52.45	12.28	4	8	15	28	47	66	86	118	155	181
				4	8	16	26	48	66	88	120	142	200
2_33	20.83	49.10	14.80	4	8	12	18	30	49	71	92	114	143
				4	9	16	25	38	56	77	99	121	147
2_52	20.93	48.51	15.30	4	7	10	16	25	34	43	58	75	90
				4	7	11	16	24	35	46	59	75	93

those used in our previous work (Foster *et al.*, 2003; Foster, Simperler *et al.*, 2004). These involve generating model SiO_2 polymorphs from the tiling nets and optimizing them using lattice energy minimization. Apart from obtaining an optimized structure for each topology, we also calculate a lattice energy, which provides an accurate guide to the thermodynamic stability that such a phase might have. A 'feasibility factor', ϑ, derived from the correlation between lattice energy and density calculated for known zeolite structure types, serves as a further measure of thermodynamic feasibility. We have also calculated the accessible volume for each pore system using a standard definition (Molecular Simulations Inc., 1999).

In describing the structural characteristics of each framework, we have resorted to the 'model building' approach (Baerlocher *et al.*, 2001; Smith, 1988; Meier, 1986; Liebau *et al.*, 1986), which is consistent with descriptions found in the online zeolite database and allows structures to be classified into 'families' if they share certain structural motifs. As part of this analysis we define as a composite building unit (CBU) every small finite unit from which a structure may be generated. These units can be corner-, edge- or face-sharing, or joined to one another by single linkages. The automated assembly of such units is also a potential method of structural enumeration, as demonstrated by Mellot-Draznieks (Mellot-Draznieks *et al.*, 2000, 2002). Zeolite structures may also be described in terms of the strictly defined secondary building units (SBUs), one type of which may be used to build a unit cell of the zeolite, without sharing T atoms. Here, we have not used the SBU approach, finding it more informative to use alternative descriptions (in general, our building units tend to be larger). However, the SBUs involved may be readily identified, as may the

Table 1 (continued)

Structure	ϑ	ΔE_{quartz} (kJ mol^{-1})	F_D (T sites per 1000 Å^3)	Coordination sequence									
2_100	22.42	45.32	19.00	4	9	18	34	58	86	113	146	194	248
				4	11	22	38	61	88	120	157	199	246
2_79	23.48	45.37	20.03	4	9	17	29	46	69	98	133	174	221
				4	10	21	37	58	84	114	148	186	229
2_77	24.27	47.94	19.04	4	9	16	26	41	61	84	110	140	175
				4	9	17	28	42	61	85	114	146	179
2_44	24.31	60.53	10.36	4	8	14	21	36	55	75	94	120	154
				4	8	16	20	34	64	72	96	128	146
2_46	24.45	57.04	12.91	4	8	14	24	36	48	64	90	118	136
				4	9	15	22	34	52	71	87	106	136
2_61	25.45	53.55	16.33	4	8	14	26	46	70	91	113	149	197
				4	10	19	30	45	68	94	122	152	186
2_22	26.31	64.37	9.70	4	7	11	18	28	42	56	68	85	111
				4	8	14	21	29	41	57	77	99	121
2_92	26.57	53.08	17.78	4	9	17	31	54	82	109	139	182	233
				4	11	22	35	55	82	110	146	188	230
2_13	26.62	61.44	12.04	4	6	15	28	34	60	69	96	126	142
				4	9	16	25	39	57	75	96	120	150
2_93	28.25	60.99	13.98	4	10	20	31	50	71	104	134	176	210
				4	9	18	30	48	70	94	134	180	213
2_12	29.67	65.74	12.11	4	6	15	20	30	50	67	90	115	126
				4	8	13	22	32	47	71	91	108	132
2_30	33.21	64.55	16.47	4	8	12	16	26	42	56	72	102	140
				4	8	13	20	30	41	56	80	111	138
2_94	33.62	58.11	21.34	4	9	18	31	55	88	121	157	194	236
				4	11	23	41	63	88	123	162	207	262
2_16	36.19	72.38	14.02	4	6	17	32	49	65	92	135	167	183
				4	11	20	28	50	81	102	117	159	222
2_34	36.28	76.83	11.03	4	8	13	19	26	38	55	74	95	115
				4	9	16	24	34	47	61	78	100	126
2_14	36.36	72.96	13.79	4	6	16	31	48	57	77	116	154	161
				4	11	19	26	42	70	93	103	128	182
2_98	37.01	63.95	20.69	4	9	18	33	51	72	105	147	184	230
				4	9	18	33	53	78	108	143	184	232
2_56	38.29	72.66	15.93	4	8	14	26	44	62	93	122	145	182
				4	11	19	29	47	68	94	123	155	193
2_116	43.29	71.75	21.56	4	11	22	39	65	96	134	175	223	280
				4	11	23	41	65	94	133	177	230	284
2_111	43.36	69.96	22.87	4	10	20	46	70	94	140	206	264	308
				4	12	25	47	74	108	155	203	262	334
2_18	44.29	89.79	10.06	4	7	10	14	17	24	37	48	57	70
				4	8	8	10	20	24	28	50	64	64
2_28	45.34	88.96	11.69	4	7	13	18	33	44	66	72	110	118
				4	8	12	21	30	50	58	82	98	138
2_15	46.13	89.89	11.83	4	12	10	28	52	34	84	124	74	172
				4	6	17	27	31	64	75	81	143	146
2_75	50.08	80.91	22.01	4	7	13	25	39	56	87	107	148	182
				4	8	14	25	40	59	84	110	147	180
2_29	50.83	93.06	14.34	4	10	18	30	45	59	103	165	219	314
				4	10	20	31	49	80	103	164	269	289
2_10	51.21	104.88	6.53	4	6	12	16	24	32	44	55	68	80
				4	6	12	17	24	31	44	55	68	82
2_5	52.01	104.95	7.28	4	5	9	14	13	16	26	34	36	44
				4	8	10	11	16	22	24	28	42	60
2_115	52.70	88.37	19.46	4	11	21	36	64	94	123	165	214	272
				4	11	23	40	63	91	126	167	213	265
2_7	53.66	105.42	8.60	4	5	10	20	26	24	44	80	98	93
				4	9	14	16	22	40	58	72	83	109
2_8	54.06	110.45	5.39	4	6	7	12	19	21	22	30	46	58
				4	8	12	13	16	22	30	36	44	56
2_6	56.38	102.26	13.51	4	5	10	19	22	25	40	62	80	90
				4	9	13	16	23	36	50	58	68	94
2_104	64.22	107.73	17.56	4	10	17	30	52	72	108	130	167	208
				4	11	20	33	52	76	105	138	173	213
2_105	65.06	106.55	19.22	4	6	9	15	28	43	65	92	134	172
				4	7	11	20	31	47	74	99	133	196
2_76	68.64	110.29	20.21	4	9	16	25	38	58	87	124	165	209
				4	10	20	34	53	78	109	146	191	245
2_63	73.83	116.23	21.28	4	8	14	27	50	80	114	153	200	258
				4	11	23	39	62	93	130	174	223	275

infinite periodic building units (PerBUs). We note that none of the units discussed are intended to represent the precursors from which zeolite crystals grow; neither do they necessarily correspond to the tiles of the original nets.

We discuss the structures in terms of the component units, and relate these to the calculated stability and feasibility. Taken together, thermodynamic feasibilty and the nature of the building units can provide a good initial guide as to which of these structures could be most readily synthesized.

2. Energy minimization

The systematically enumerated nets (Delgado Friedrichs *et al.*, 1999) were first converted into atomistic models. This was done by inserting an Si atom at each vertex point in the network and placing a bridging oxygen between each pair of adjacent Si atoms. Each net was scaled such that the vertices were separated by *ca* 3.1 Å, a typical Si—Si distance. The resulting structure was then pre-optimized using the DLS (distance least squares) method (Meier & Villiger, 1969), which performs geometric refinement of the structure by fitting bond lengths and angles to the prescribed values, and reduces the amount of computer time needed for the subsequent minimization of lattice energy. This procedure was found to have no influence on the final result: using lattice energy minimization from the outset gives the same structure, but at greater computational expense. The lattice energy and crystallographic data are those extracted from the GULP minimizations, whereas coordination sequences, bond distances and angles were calculated with *zeoT-sites* (Version 1.2; Sastre & Gale, 2001). The connectivity was additionally checked with the software tool *KRIBER* (Version 1.1; Bialek, 1995). Additional calculations were carried out using *Cerius*^{2} software (Molecular Simulations Inc., 1999).

Table 1 (continued)

Structure	ϑ	ΔE_{quartz} (kJ mol^{-1})	F_D (T sites per 1000 Å^3)	Coordination sequence									
2_9	73.85	127.41	13.56	4	6	8	14	20	30	45	54	73	98
				4	7	10	14	22	34	42	58	78	94
2_60	79.89	131.67	16.65	4	8	14	26	45	68	93	125	171	223
				4	11	22	35	52	76	109	148	189	232
2_80	87.12	142.73	16.21	4	9	17	29	48	70	100	138	175	222
				4	11	20	36	58	81	112	146	189	240
2_42	104.27	164.99	17.94	4	8	14	21	32	48	67	91	117	149
				4	10	18	28	42	59	80	105	134	168
2_4	107.62	186.37	6.48	4	5	8	16	18	24	36	48	63	72
				4	8	10	15	22	26	38	54	64	80
2_36	166.29	262.64	12.30	4	8	13	20	29	41	56	72	89	110
				4	9	16	24	33	44	58	76	97	120
2_69	189.35	292.92	14.38	4	8	17	29	46	68	91	117	154	184
				4	9	17	28	49	69	92	119	151	184

Structural figures were prepared using *GDIS* (SourceForge, 2004) and *POV-Ray* (Persistence of Vision Raytracer Pty. Ltd, 2004; Henson *et al.*, 1994). The lattice energy, ΔE_{quartz}, given in Table 1, is relative to that of α-quartz, calculated using the same potential model, and is thus analogous to the heat of transition reported for several high-silica zeolites (Henson *et al.*, 1994; Petrovic *et al.*, 1993; Navrotsky *et al.*, 1995; Hu *et al.*, 1995; Piccione *et al.*, 2000, 2001, 2002; Moloy *et al.*, 2002).

2.1. The feasibility factor

The well established relationship between framework density and calculated lattice energy (Foster *et al.*, 2001, 2003; Foster, Friedrichs *et al.*, 2004; Foster, Simperler *et al.*, 2004; Simperler *et al.*, 2004) was confirmed experimentally (Henson *et al.*, 1994) for known zeolites. Using the standard least-squares technique, a straight line was fitted to 145 data points obtained from minimizing quartz and all the known zeolite topologies in a purely siliceous form (Fig. 1). We excluded the four non-silicate structure types which substantially deviate from the rest: WEI (calcium beryllophosphate), CZP (sodium zincophosphate), OSO (potassium berylosilicate) and RWY (gallium germanium sulfide). The line of best fit has the formula $y = -1.4433x + 40.3904$, where x is the framework density (F_D) and y is ΔE_{quartz}. The feasibility factor, ϑ, is then simply the dimensionless deviation of a data point (x_1, y_1) from the line of best fit, given by the vertical offset $\vartheta = \left|1.4433x_1 + y_1 + 40.3904\right|/1.4433$. Being formally independent of the framework density, the feasibility factor ϑ is thus a convenient way of discriminating between candidate structures and can be compared with the values obtained from known zeolite structures. We minimized all the known zeolite topologies as silica polymorphs, regardless of the actual composition in which they occur. We believe that ϑ is a better gauge of the feasibility of the structure than ΔE_{quartz} alone, as evidenced by the fact that seven of the ten lowest ϑ values in Table 1 belong to structures with known zeolite topologies. A ranking in order of ascending ΔE_{quartz} would, in contrast, produce only four values. Virtually all of the topologies which are known in the form of silicates, aluminosilicates or aluminophosphates, including those with low levels of heteroatom substitution, have $\vartheta < 5$. This reflects the similarity of the preferred geometry between (alumino)silicates and AlPOs. The highest values of ϑ are 5.03 for AFY (Co-AlPO-50), which has 19% framework cobalt, and 5.18 for AHT, only known as the thermally unstable material AlPO-H2. By analogy, we define structures with $\vartheta < 5$ as feasible 'conventional' zeolites, *i.e.* those for which natural zeolites along with high-silica and AlPO forms are known. Framework types with more 'exotic' compositions have $\vartheta > 5$. For example, the zincosilicates VNI, VSV and RSN have ϑ of 5.75, 6.07 and 6.09, respectively. Beryllosilicates, generally containing three rings, also have higher ϑ, *e.g.* LOV (6.51), NAB (10.99) and OSO (23.30), while the beryllophosphate weinebeneite has ϑ = 12.24 and the zincophosphate CZP ϑ = 20.92. We therefore propose that ϑ values up to 25 indicate that the topology may be feasible in the form of an 'oxide' material. Above this, we note that for RWY, the only zeotype structure known solely as a framework sulfide, ϑ = 51.69. Many other compositions, such as metal-organic frameworks, are of course possible. This means that although a structure may be deemed highly unfeasible as a zeolite, it may exist in other chemical forms. Also, the precise value of ϑ will be an unreliable guide in the high region, since it is based only on a silica model. In order to gauge the feasibility of a particular topology in a different composition, it would be necessary to carry out separate series of computations, taking into account the actual composition.

The *Cerius*^{2} software suite (Molecular Simulations Inc., 1999) was used for visualizing and manipulating the structures and for calculating free volumes, space-group symmetry and other parameters. In addition to calculating the energetics of the hypothetical structures, it is important to compare the calculated values with the values for all known zeolite frameworks. Thus, all relevant properties were also calculated for the purely siliceous forms of all known zeolite topologies. Lattice energies were calculated relative to α-quartz, the most stable form of the mineral at ambient temperature.

The 'available volume', defined as the difference between the volume of the unit cell and the effective volume of all the atoms, depends on the van der Waals radius used for each atom. 'Occupiable volume' is the volume which can be occupied by a probe molecule with a given radius as it probes the surface of the structure. The 'accessible volume' is determined by tracing out the volume by the centre of the probe molecule as it follows the structure contours, but with the extra requirement that the probe must enter the unit cell from the outside *via* sufficiently wide pores or channels. The accessible volume gives an indication of the space available within each

structure for applications in molecular sieving and catalysis. The calculations of the accessible volume were performed using the Free Volume module of the *Cerius*[2] package, which applies the Connolly (1985) method consisting of 'rolling' a probe molecule with a given radius over the van der Waals surface of the framework atoms. We have used a probe molecule with a radius of 1.4 Å (such as water) and 1.32 and 0.9 Å for the radii of O and Si atoms, respectively. The void volume, enclosed within the Connolly surface, was calculated first. The accessible volume was then calculated by requiring the probe molecule to enter the unit cell from the outside.

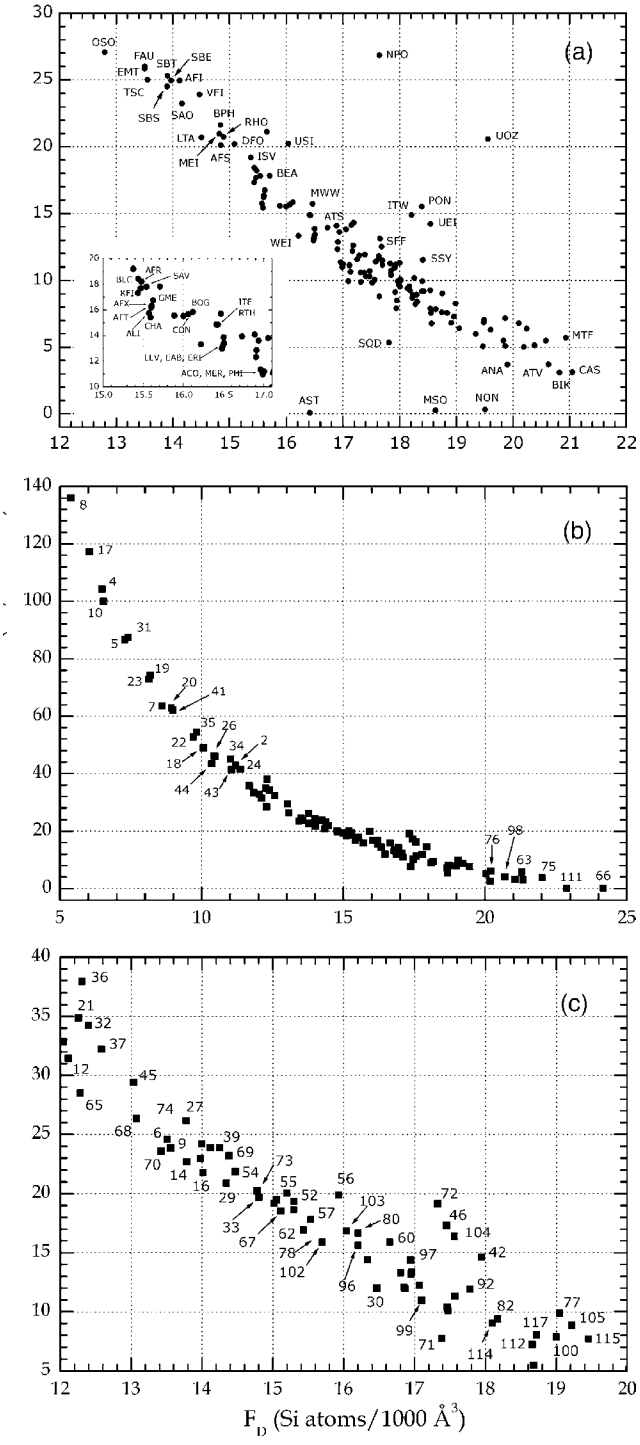

Figure 2
Accessible volume (Å^3 per Si atom) *versus* framework density for (*a*) all known zeolitic structure types; (*b*) hypothetical binodal zeolitic structures; (*c*) structures with accessible volumes below 40 Å^3 per Si atom.

3. Results and discussion

Of the 117 structures, eight could not be optimized, either because refinement was not possible or because of failure during minimization, usually resulting in loss of the original network topology. The remaining 109 structures are described below. For the most part, these minimized smoothly without any loss of symmetry, although there are a few whose low-energy symmetry is lower than that of the original space group. In these instances, the original space group is shown in parentheses in Table 2.

Figs. 1(*a*) and (*b*) show plots of framework energy relative to α-quartz, E_F, *versus* the framework density, F_D, for all known zeolites. Relative framework energies of the hypothetical binodal frameworks range from 11.15 kJ mol^{-1} (structure 2_114) to as much as 515.43 kJ mol^{-1} (structure 2_72) (Fig. 1*c*). Fig. 1(*d*) plots the framework energy *versus* the framework density for the hypothetical binodal structures with energies below 30 kJ mol^{-1}, the range considered as the most 'desirable', and with framework densities typical of the known zeolites.

Fig. 2(*a*) shows a plot of accessible volume *versus* framework density for the known structural types and Figs. 2(*b*) and (*c*) the corresponding plot for hypothetical binodal zeolites. Low framework density structures are of particular interest as they have very high accessible free volumes. Of the structures with framework densities below 18 Si atoms/1000 Å^3, structures 2_57, 2_58, 2_59, 2_82, 2_85, 2_86, 2_87, 2_91, 2_95, 2_96, 2_102, 2_103, 2_106, 2_108, 2_109, 2_110, 2_112, 2_113, 2_114 and 2_117 are energetically stable (Fig. 1*c*). Many hypothetical structures have dense frameworks, which are largely inaccessible. However, as many known zeolite topologies have low accessible volumes (Fig. 2*a*), a structure cannot be ruled out as a feasible topology on the basis of a low accessible free volume, even though it may be of no interest to scientists studying sorption, ion exchange or catalysis. A plot of framework density for known zeolites and for dense silicate frameworks against the size of the smallest ring in the structure (Brunner & Meier, 1989) shows that very open frameworks with low F_D have the largest number of four- and three-membered rings and that there is a gap in F_D between compact minerals, such as quartz and tridymite, and the zeolite frameworks. The lower boundary of F_D for known zeolites is from about 11 tetrahedral atoms per 1000 Å^3 in materials with four-membered rings to about 17 tetrahedral atoms in materials with 5+ rings, where the plus sign signifies that some tetrahedral atoms are associated only with the larger rings.

Fig. 3 plots the framework energy with respect to α-quartz for the known zeolitic structures and the hypothetical binodal structures *versus* the accessible volume, thus combining

information contained in Figs. 1 and 2. Structures of the greatest practical interest are those with low energies and large volumes (see inset in Fig. 3*b*). Full details of all the structures have recently been published elsewhere (Foster, Simperler *et al.*, 2004). Crystallographic CIF files from which powder X-ray diffraction patterns can be easily calculated are given as supplementary information.[1]

The structures have been divided into 15 families, the members of which share a common building scheme or structural unit. As explained above, the building units used do not necessarily equate to SBUs or PerBUs in the strict sense. We also note that the allocation of a structure to a certain family is not unequivocal: there are several structures which could equally well be assigned to more than one family. The order in which the various families are discussed is dictated by the feasibility factor of the most feasible structure in that family. Selected members of a particular family are shown in Figs. 4–9 in the same order, whereas a full description of all members is available in the electronic supplement. The more feasible structures will thus be encountered earlier in the following sections, with the exception of the 'orphan family' which contains several chemically feasible members. In describing the various structures, we use standard nomenclature from the zeolite literature. For instance, 'D6R' refers to a double six-ring unit. In describing polyhedral cages or units, the $[M^xN^y]$ system adopted by Smith (1988) is also used, where (M, N) is the number of edges defining a given face and (x, y) is the number of times that face appears in the polyhedron. Results are also tabulated in Table 1 (in order of ϑ) and Table 2 (in numerical order of the structures). Table 1 gives ϑ, $\Delta E_{\rm quartz}$, the framework density and the coordination sequences of the T sites. Table 2 gives the crystallographic data.

3.1. ABC-6 family

Of the 109 refinable binodal structures, 13 can be described using the building scheme for the ABC-6 family (van Koningsveld, 2004). Six of these are known frameworks: 2_89 = ERI, 2_84 = EAB, 2_90 = SAT, 2_83 = LEV, 2_107 = LOS and 2_78 = AFX. The PerBU of the family consists of a hexagonal array of isolated six-membered rings, which are related by pure translations along [100] and [010]. A three letter code (*A*, *B* and *C*) gives the connection mode of the layers along [001]. The six-membered rings of *A* are centred at (0,0), while layer *B* is shifted by (+2/3*a*,+1/3*b*) and layer *C* by (+1/3*a*,+2/3*b*). The connection between six-rings in adjacent layers is invariably *via* four-rings. In the (001) projection, there is a close similarity between all the structures of this family, epitomized by that of 2_106 (Fig. 4*a*), where the hexagonal array of six-rings, interspersed by four-rings, is clearly evident. Each structure is uniquely characterized by its [001] stacking sequence and the stacking sequences of the 13 structures (in order of their 'thermodynamic feasibility') are *ABBACBBC*(*A*) for 2_87, *ACAABA*(*A*) for 2_89 (ERI), *ACCABB*(*A*) for 2_84 (*EAB*), *AABABBCBCCAC*(*A*) for 2_90 (SAT), *ABBC*(*A*) for 2_86, *AACBBACCB*(*A*) for 2_83 (LEV), *ABAC*(*A*) for 2_107 (LOS), *ACABABCBC*(*A*) for 2_110, *ACABCB*(*A*) for 2_106, *ACACBABACBCB*(*A*) for 2_108, *ACCAABBA*(*A*) for 2_78 (AFX), *ACCCBBBAA*(*A*) for 2_40, and *AAAACCCCBBBB*(*A*) for 2_33. 2_87, 2_89, 2_84, 2_107, 2_106 and 2_78, which have hexagonal symmetry, space group $P6_3/mmc$, while 2_90, 2_83, 2_110, 2_108, 2_40 and 2_33 (all $R\bar{3}m$) and 2_86 ($P\bar{3}m1$) are trigonal. The ABC-6 structures, both known and hypothetical, are among the most thermodynamically favoured as silica polymorphs and, as can be seen from Table 1, have high chemical feasibilities ($0.08 < \vartheta < 0.98$), except for 2_40 and 2_33 which have ϑ of 14.97 and 20.83, respectively. The ABC-6 structures may also be thought of in terms of stacks, or chains, of cages linked parallel to the [001] direction through six-rings and, depending on symmetry, there are either one or two distinct types of stack. For example, the most feasible structure 2_87 (Figs. 4*b* and *c*) contains both the $[4^96^28^3]$ gmelinite cages and $[4^96^88^3]$ EAB cages, which alternate along (001) (Fig. 4*c*). Parallel to these are stacks of alternating sodalite cages and double six-rings

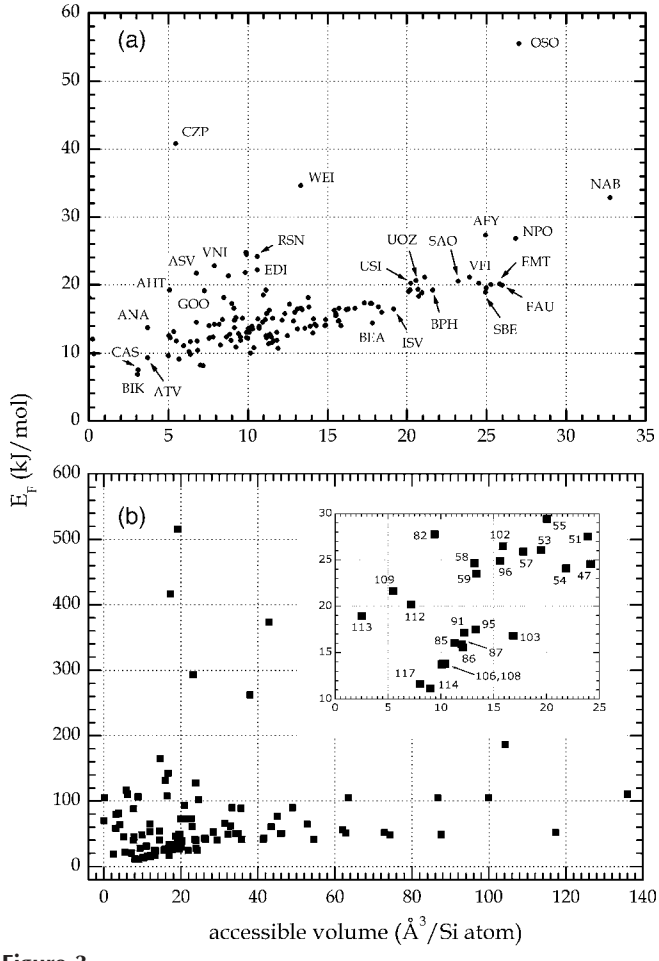

Figure 3
Framework energy with respect to α-quartz *versus* accessible volume (Å^3 per Si atom) for (*a*) all known zeolitic structure types; (*b*) hypothetical binodal zeolitic structures. Hypothetical structures of particular chemical interest are identified in the inset.

[1] Supplementary data for this paper are available from the IUCr electronic archives (Reference: BK5018). Services for accessing these data are described at the back of the journal.

Table 2
Space groups and unit-cell dimensions of 109 hypothetical binodal zeolites, optimized as purely siliceous structures.

Structure	Space-group symbol	Space-group number	a (Å)	b (Å)	c (Å)	α (°)	β (°)	γ (°)
2_4	$Im\bar{3}m$	229	24.5550	24.5550	24.5550	90	90	90
2_5	$Im\bar{3}m$	229	23.6252	23.6252	23.6252	90	90	90
2_6	$Pn\bar{3}m$	224	19.2265	19.2265	19.2265	90	90	90
2_7	$P\bar{4}3m$	215	14.0784	14.0785	14.0785	90	90	90
2_8	$Im\bar{3}m$	229	29.9045	29.9046	29.9046	90	90	90
2_9	$R\bar{3}m$	166	20.6871	20.6871	10.7470	90	90	120
2_10	$Im\bar{3}m$	229	30.8610	30.8610	30.8610	90	90	90
2_12	$I4_1/amd$	141	15.1769	15.1769	17.2033	90	90	90
2_13	Fm/m	225	17.4521	17.4521	17.4521	90	90	90
2_14	$I4/mmm$	139	11.5929	11.5929	12.9540	90	90	90
2_15	Pm/n	223	13.6367	13.6367	13.6367	90	90	90
2_16	$P4_2/mnm$	136	10.2171	10.2171	16.3964	90	90	90
2_17	$Im\bar{3}m$	229	31.6666	31.6666	31.6666	90	90	90
2_18	$Im\bar{3}m$	229	18.1332	18.1332	18.1332	90	90	90
2_19	$Im\bar{3}m$	229	26.0211	26.0211	26.0211	90	90	90
2_20	$Pm\bar{3}m$	221	17.5191	17.5191	17.5191	90	90	90
2_21	$Fm\bar{3}m$	225	31.5256	31.5256	31.5256	90	90	90
2_22	$Pm\bar{3}m$	221	19.5087	19.5087	19.5087	90	90	90
2_23	$Fm\bar{3}m$	225	32.8255	32.8255	32.8255	90	90	90
2_24	$Pm\bar{3}m$	221	14.6896	14.6986	14.6896	90	90	90
2_25	$Fm\bar{3}m$	225	30.1897	30.1897	30.1897	90	90	90
2_26	$Fm\bar{3}m$	225	30.2151	30.2151	30.2151	90	90	90
2_27	$Fm\bar{3}m$	225	27.5480	27.548	27.5480	90	90	90
2_28	$Im\bar{3}$	204	16.0155	16.0155	16.0155	90	90	90
2_29	$Fd\bar{3}c$	228	29.9172	29.9172	29.9172	90	90	90
2_30	$Pn\bar{3}m$	224	15.3879	15.3879	15.3879	90	90	90
2_31	$R\bar{3}m$ ($Fd\bar{3}m$)	166 *(227)*	26.3028	26.3028	64.9314	90	90	120
2_32	$Im\bar{3}m$	229	24.9270	24.9270	24.9270	90	90	90
2_33	$R\bar{3}m$	166	13.1741	13.1741	32.3570	90	90	120
2_34	$Im\bar{3}m$	229	25.9183	25.9183	25.9183	90	90	90
2_35	$Fd\bar{3}m$	227	30.8413	30.8416	30.8413	90	90	90
2_36	$Pm\bar{3}m$	221	19.8342	19.8342	19.8342	90	90	90
2_37	$Pn\bar{3}m$	224	19.6887	19.6887	19.6887	90	90	90
2_39	$P1$ ($Im\bar{3}m$)	1 *(229)*	21.5940	21.6260	21.6370	90.1262	89.9558	90.0775
2_40	$R\bar{3}m$	166	13.2084	13.2084	23.8034	90	90	120
2_41	$Im\bar{3}m$	229	25.2127	25.2127	25.2127	90	90	90
2_42	$Im\bar{3}m$	229	20.0209	20.0209	20.0209	90	90	90
2_43	$Fm\bar{3}m$	225	25.9040	25.9040	25.9040	90	90	90
2_44	$P\bar{4}3m$	215	11.3123	11.3124	11.3124	90	90	90
2_45	$Pm\bar{3}m$	221	17.6786	17.6786	17.6786	90	90	90
2_46	$Pn\bar{3}m$	224	15.4919	15.4919	15.4919	90	90	90
2_47	$Pm\bar{3}m$	221	19.0003	19.0003	19.0003	90	90	90
2_48	$Pm\bar{3}n$	223	16.7613	16.7613	16.7613	90	90	90
2_50	$P\bar{3}1m$	162	12.3351	12.3351	8.6007	90	90	120
2_51	$P6_3/mcm$	193	12.3340	12.3340	17.2043	90	90	120
2_52	$Pn\bar{3}m$	224	16.7584	16.7584	16.7584	90	90	90
2_53	$Pn\bar{3}m$	224	18.5448	18.5448	18.5448	90	90	90
2_54	$I4/mmm$	139	14.8438	14.8438	20.0782	90	90	90
2_55	$P6_3/mcm$	193	13.7562	13.7562	19.2727	90	90	120
2_56	$P\bar{3}1m$	162	13.7003	13.7003	9.2686	90	90	120
2_57	$I4/mmm$	139	14.0993	14.0993	15.5435	90	90	90
2_58	$I4/mmm$	139	13.5265	13.5265	20.6385	90	90	90
2_59	$P4/nmm$	129	13.5133	13.5133	10.3319	90	90	90
2_60	$Im\bar{3}m$	229	17.9320	17.9320	17.9320	90	90	90
2_61	$I4_1/amd$	141	16.3875	16.3875	10.9441	90	90	90
2_62	$Pm\bar{3}m$	221	14.5985	14.5985	14.5985	90	90	90
2_63	$I\bar{4}m2$	119	12.6142	12.6142	9.4486	90	90	90
2_64	$Pm\bar{3}m$	221	18.3419	18.3419	18.3419	90	90	90
2_65	$Ia\bar{3}$	206	18.0311	18.0311	18.0311	90	90	90
2_67	$Ia\bar{3}d$	230	19.9520	19.9520	19.9520	90	90	90
2_68	$I4_1/amd$	141	15.1043	15.1043	10.7274	90	90	90
2_69	$R\bar{3}m$	166	16.6853	16.6853	20.9554	90	90	120
2_70	$Pm\bar{3}m$	221	13.8940	13.8940	13.8940	90	90	90
2_71	$P2_13$	198	14.0298	14.0298	14.0298	90	90	90
2_73	$Fd\bar{3}m$	227	29.6184	29.6184	29.6184	90	90	90
2_74	$Fm\bar{3}m$	225	30.4872	30.4872	30.4872	90	90	90
2_75	$Fd\bar{3}m$	227	25.9368	25.9368	25.9368	90	90	90
2_76	$P\bar{4}3m$	215	13.3418	13.3418	13.3418	90	90	90
2_77	$Pn\bar{3}m$	224	15.5787	15.5787	15.5787	90	90	90

(D6R). The structure 2_40, which is less dense, is quite interesting as it has large cages linked through elongated 10- and 12-rings, respectively (Fig. 4*d* and *e*).

3.2. [$3^2 5^6$] family

Four structures (2_103, 2_55, 2_56 and 2_104) are built up from columns of [$3^2 5^6$] polyhedral units (Fig. 4*g*) arranged hexagonally so as to give 12-membered ring channels along the *c* direction (Fig. 4*f*). The [$3^2 5^6$] units are linked by sharing their 'terminal' three-membered ring windows (Fig. 4*h*) in structures 2_103 and 2_104, while in structures 2_55 and 2_56 these small cage units are separated by a [$3^2 4^3$] unit (*i.e.* a trigonal prism or D3R; Fig. 4*i*). None of these four are known structures, although 2_103 is expected to be highly chemically feasible (ϑ = 0.30). Three further members of this family, 2_112, 2_102 and 2_80, also contain the [$3^2 5^6$] unit (Fig. 4*g*), but with different building patterns. For example, in 2_112 the [$3^2 5^6$] units are linked *via* single oxygen bridges, while in 2_102 and 2_80 the units are linked *via* double oxygen bridges (Fig. 4*j*). Both 2_112 and 2_102 are highly feasible, with ϑ = 4.66 and 6.08, respectively, as opposed to 2_80 which has ϑ = 87.12.

3.3. AWW family

The nine structures which we describe as members of the 'AWW family' share a small [$4^6 6^4$] cage as the common building unit (Fig. 5*a*). Six of these structures, 2_88 (which has the actual AWW topology), 2_85, 2_59, 2_58, 2_100 and 2_63, are tetragonal, with columns of larger cages parallel to [001] and having eight-ring windows as the maximum pore diameter in that direction. The archetypal example is the AWW [$4^8 6^8 8^2$] cage (Fig. 5*b*), which stacks through shared eight-rings. Fig. 5(*c*) shows the [001] projection of 2_85, which is typical of this series.

Depending on the linkage pattern of the [$4^6 6^4$] building units along [001], different types of large cage are defined. AWW, 2_59, 2_100 and 2_63

Table 2 (continued)

Structure	Space-group symbol	Space-group number	a (Å)	b (Å)	c (Å)	α (°)	β (°)	γ (°)
2_78	$P6_3/mmc$	194	13.5479	13.5479	19.3503	90	90	120
2_79	$Im\bar{3}m$	229	21.2424	21.2424	21.2424	90	90	90
2_80	$Im\bar{3}m$	229	18.0938	18.0938	18.0938	90	90	90
2_81	$I4/mmm$	139	13.9993	13.9993	10.2051	90	90	90
2_82	$Pn\bar{3}m$	224	15.8240	15.8240	15.8240	90	90	90
2_83	$R\bar{3}m$	166	12.9786	12.9786	22.4610	90	90	120
2_84	$P6_3/mmc$	194	12.9887	12.9887	14.9436	90	90	120
2_85	$I4/mmm$	139	13.2812	13.2812	15.4875	90	90	90
2_86	$P\bar{3}m1$	164	12.7931	12.7931	10.0490	90	90	120
2_87	$P6_3/mmc$	194	12.7982	12.7982	20.0706	90	90	120
2_88	$P4/nmm$	129	13.5200	13.5199	7.6115	90	90	90
2_89	$P6_3/mmc$	194	12.9122	12.9122	15.1051	90	90	120
2_90	$R\bar{3}m$	166	12.7260	12.7259	30.3678	90	90	120
2_91	$I4/mcm$	140	13.9768	13.9768	19.1953	90	90	90
2_92	$P4/nbm$	125	13.9490	13.9490	9.2497	90	90	90
2_93	$Im3m$	229	17.2697	17.2697	17.2697	90	90	90
2_94	$C2$ ($Fd\bar{3}m$)	5 *(227)*	29.4382	29.3841	20.7989	90	90	90
2_95	$I4/mmm$	139	12.2058	12.2058	19.1794	90	90	90
2_96	$Im\bar{3}$	204	16.4413	16.4413	16.4413	90	90	90
2_97	$Pm3n$	223	16.1973	16.1973	16.1973	90	90	90
2_98	$P4_132$	213	11.5642	11.5642	11.5642	90	90	90
2_99	$Pm3$	200	12.8171	12.8171	12.8171	90	90	90
2_100	$I\bar{4}m2$	119	12.8690	12.8691	7.6292	90	90	90
2_101	$Fm3m$	225	13.4592	13.4592	13.4592	90	90	90
2_102	$R\bar{3}m$	166	12.6141	12.6141	16.6417	90	90	120
2_103	$P6_3/mcm$	193	13.6152	13.6152	13.9813	90	90	120
2_104	$P\bar{3}1m$	162	13.4810	13.4810	6.5129	90	90	120
2_105	$P1$ ($R\bar{3}c$)	1 *(167)*	10.6747	16.8789	16.9018	67.8079	86.0781	86.1532
2_106	$P6_3/mmc$	194	12.4093	12.4093	15.4571	90	90	120
2_107	$P6_3/mmc$	194	12.3972	12.3972	10.3205	90	90	120
2_108	$R\bar{3}m$	166	12.4186	12.4186	30.8573	90	90	120
2_109	$Pn\bar{3}m$	224	17.2562	17.2562	17.2562	90	90	90
2_110	$R\bar{3}m$	166	12.4060	12.4060	23.1948	90	90	120
2_111	$P4_132$	213	11.6324	11.6324	11.6324	90	90	90
2_112	$P2_13$	198	13.7019	13.7019	13.7019	90	90	90
2_113	$Fddd$	70	7.4170	13.5469	23.6645	90	90	90
2_114	$I4/mcm$	140	13.7055	13.7055	14.1225	90	90	90
2_115	$P4/nbm$	125	13.4128	13.4128	6.8567	90	90	90
2_116	$I432$	211	16.4510	16.4519	16.4510	90	90	90
2_117	$P4_2/mnm$	136	7.1839	7.1839	12.4079	90	90	90

have only one type of eight-ring channel cage each, whilst in 2_85 two alternating types of larger cage are thus defined, $[4^8 6^{12} 8^2]$ and $[4^8 6^4 8^2]$ (also found in the structures SAS and ATN respectively). Structures AWW, 2_58, 2_59 and 2_85 fall within the feasible range, with ϑ = 0.32–6.04, while 2_100 (ϑ = 22.42) and 2_63 (ϑ = 73.83) are less feasible.

There are also three cubic structures, which contain the same building unit (2_109, 2_97 and 2_60), with 2_109 being by far the most feasible of the three (ϑ = 5.67). For these three structures, the $[4^6 6^4]$ units alternate with sodalite or beta cages in a chain along [100]. Structure 2_97 (ϑ = 16.99) falls within the extended range of oxide feasibility, whereas 2_60 (ϑ = 80.04) does not.

3.4. Supercage family

There are 11 structures which contain sodalite or LTA (alpha) cages linked by smaller prismatic units in such a way that it also generates much larger cages. All the structures have cubic or pseudo-cubic symmetry, as can be seen in the [100] view of 2_45 (Fig. 5*e*). Structure 2_74 has the framework of the mineral tschörtnerite (TSC) with both sodalite and alpha cages linked *via* D6R (Fig. 5*f*), thus defining the large TSC cage (Fig. 5*g*). The remaining structures will be discussed with respect to structural similarities and not by their chemical feasibility factor, ϑ.

Structures 2_35 (Fig. 5*h*) and 2_31 are composed of sodalite cages linked tetrahedrally *via* D6R and thus form a series together with the FAU structure. 2_35 and 2_31 are both feasible as oxide materials, with ϑ of 10.69 and 13.16, respectively. 2_45 (Fig. 5*i*) and 2_36 can similarly be imagined as belonging to a series with RHO, a structure formed by alpha cages linked octahedrally *via* D8R. Both have $Pm\bar{3}m$ symmetry and 2_45 is relatively feasible (ϑ = 12.91). 2_24 (Fig. 5*j*) and 2_20 are related to the LTA structure, since they can be generated by linking sodalite cages and D4R. They also have the same supercages as 2_45 and 2_36 and similar ϑ of 13.28 and 16.11, respectively. Structures 2_27 (Fig. 7*k*) and 2_21 can also be considered part of a series with LTA, except in this case it is the alpha cages which are retained and the linkages between them expanded. The final pair, 2_39 (Fig. 5*l*) and 2_32, form a series derived from KFI, containing alpha cages which are connected *via* shared D6R and are replaced by stacks of two and three D6R.

3.5. SAS family

These structures are analogous to the AWW family as they contain stacks of large cages linked unidirectionally by eight-rings. Fig. 6(*a*) shows the [001] projection of structure 2_54, typical of all four tetragonal structures belonging to this family and having $I4/mmm$ space-group symmetry [2_54, 2_57, 2_81 (SAS) and 2_95]. The basic building units may be thought of as smaller polyhedra arranged in parallel chains: in the case of 2_81 the basic units are D6R hexagonal prisms, which form a chain by sharing four-rings, 2_95 is a highly feasible (ϑ = 0.93) structure in which $[4^4 5^4]$ units are linked into chains *via* four-rings (Fig. 6*b*); in 2_57 an additional D4R is interposed between the alternating D6R and 2_54 is built analogously from chains of alternating D8R and D4R. Aside from SAS and 2_95, both 2_54 and 2_57 are also quite feasible as zeolites (ϑ = 3.18 and 5.51, respectively).

3.6. [$4^2 5^8$] family

These structures have a small [$4^2 5^8$] cage as the building unit (Fig. 6*d*). In four of the structures, these units are linked into chains through the four-rings which cap the cages. The structures are tetragonal with [$4^2 5^8$] chains running along [001] and have large cages accessible through eight-rings. The projection of 2_91 along [001] is typical of this family (Fig. 6*c*). Structure 2_91 is the most feasible of these structures (ϑ = 0.95) and has [$4^2 5^8$] cages linked through D4R, with a chain repeat motif of two cages and two D4R. In 2_114, another highly feasible structure with ϑ = 2.17, the cages are directly linked through a shared four-ring. Structures 2_92 and 2_115 are analogous to structures 2_91 and 2_114, respectively, but with only half the chain repeat distance. Both structures are far less feasible, as is a fifth structure, 2_116 (Figs. 6*e* and *f*), in which the [$4^2 5^8$] units are linked into chains *via* pairs of $T-O-T$ linkages (Fig. 6*f*). In the latter, the chains are interconnected so as to run in all three directions of the cubic lattice and the structure also contains sodalite cages, each of which shares its four-ring windows with [$4^2 5^8$] units.

3.7. AST family

Structure 2_101 (Fig. 6*g*–*i*) is topologically identical to the known zeolite AST (AlPO-16).[33,34] The structure contains the characteristic [$4^6 6^{10}$] cages (Fig. 6*i*), but may also be thought of in terms of D4R units connected through $O-T-O$ bridges (Fig. 6*h*). In 2_73 the D4R connect through single oxygen bridges and, apart from containing sodalite cages, the structure also possesses large tetrahedral cages with 12-ring apertures. Structure 2_61 is tetragonal containing cages with oval-shaped ten-rings as their largest apertures. Topologically, 2_13 (Figs. 6*j* and *l*) is a variation of the AST structure in which those *T* atoms which *do not* form part of D4R are replaced by the [3^4] tetrahedra of *T* sites, a structural feature not found in aluminosilicate zeolites, although present, for instance, in the zeotypic sulfide RWY.

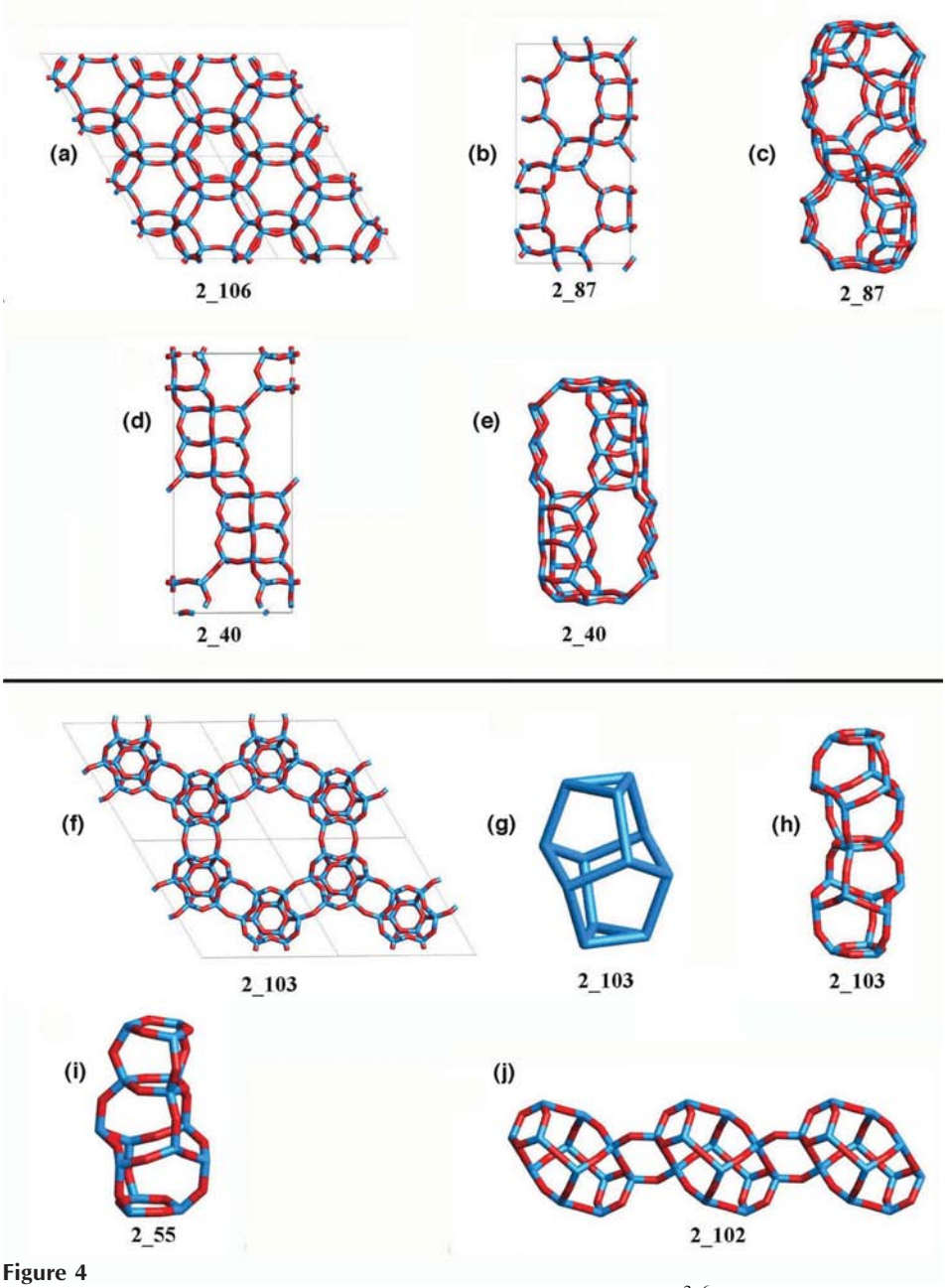

Figure 4
Molecular graphic illustrations of some structures from the ABC-6 and [$3^2 5^6$] families.

3.8. D8R family

This family is formed by four structures which contain the double eight-ring (D8R) as a structural unit. Structure 2_47 has a cubic structure in which the building unit may be thought of as a D8R with four D4R attached to alternate four-ring faces (Fig. 7*a*). The units do not link directly to one another, but are arranged so as to define the large [$4^{24} 6^8 8^{18}$] (TSC) cages (Fig. 7*b*). Structures 2_19 and 2_17 form part of a homologous series of structures, together with the uninodal structure 1_11 (Foster *et al.*, 2003), one of the nine simple uninodal tilings. The latter structure has a body-centered cubic framework based on chains of D8R and D4R, and 2_19 has the same structure, except that the D4R in 1_11 are replaced in 2_19 by pairs of face-sharing D4R (Fig. 7*c*) and

in 2_17 by groups of three D4R. The more complex 2_34 structure also contains the D8R/D4R units, but with the addition of $[4^6 6^4]$ AWW cages forming large cages with 12-rings as the maximum aperture (Fig. 7*d*). Topologically, the tile which corresponds to this cage is the largest among this set of binodal frameworks, with 74 faces, 144 vertices and 216 edges. Structure 2_34 shares the space group $Im\bar{3}m$ with both 2_19 and 2_17. Structure 2_47 is thermodynamically feasible (ϑ = 3.02), while 2_17 and 2_19 have ϑ = 13.96 and 13.39, respectively, despite having extremely low framework densities of 8.17 and 6.05*T* per 1000 Å^3, respectively.

3.9. AFY family

Structure 2_50 is topologically identical to the known structural type AFY (AlPO-50). The secondary building unit of this family is a D4R, which in AFY form hexagonal layers (Fig. 7*e*) and are tilted with respect to the (001) plane. These layers then repeat through simple translation along *c*, most clearly seen in the (120) projection (Fig. 7*f*; van Koningsveld, 2004; Baelocher & McCusker, 2004). If, instead, the layers alternate in orientation by means of a mirror plane (*i.e. ABA* rather than *AA*), the hypothetical framework 2_51 is formed. Both have low ϑ values: 5.03 and 5.18 for 2_50 and 2_51, respectively, making 2_51 virtually as feasible as AFY.

3.10. D6R family

This family comprises seven structures (2_6, 2_30, 2_53, 2_75, 2_76, 2_77 and 2_82) which have in common D6R hexagonal prisms as building units. These structures are all cubic, space group $Pn\bar{3}m$, with the exception of 2_76 and 2_75, for which D6R (*i.e.* 6–6) may be strictly defined as a secondary building unit. The first five members of the group may be thought of in terms of chains running along [110] in which the D6R are linked by various combinations of rings. In the most feasible member of the family, 2_53 (ϑ = 5.11), the link unit includes D4R, giving rise to the characteristic motif shown in Fig. 7(*g*), where four D6R are connected to a single D4R. This structure also contains FAU supercages linked *via* the $[4^{18}8^6 12^2]$ cages (Fig. 7*h*). Structure 2_82 is quite similar to 2_53, whereas in 2_77 the D6R chains are linked by units of three four-rings and in 2_30 a spiro-5 unit links the D6R into chains. Structure 2_6 also contains three-rings linked into $[3^4]$ tetrahedra which connect the D6R. Finally, structures 2_75 and 2_76 are the 'odd ones' of the family since it is not possible to describe them using the D6R chain model. Structure 2_75 is very unusual as it contains both 'regular' and flattened sodalite cages connected through six-rings (Fig. 7*i*). Structure 2_76 contains (differently) distorted beta cages as well as larger cages accessible through both approximately planar six-rings

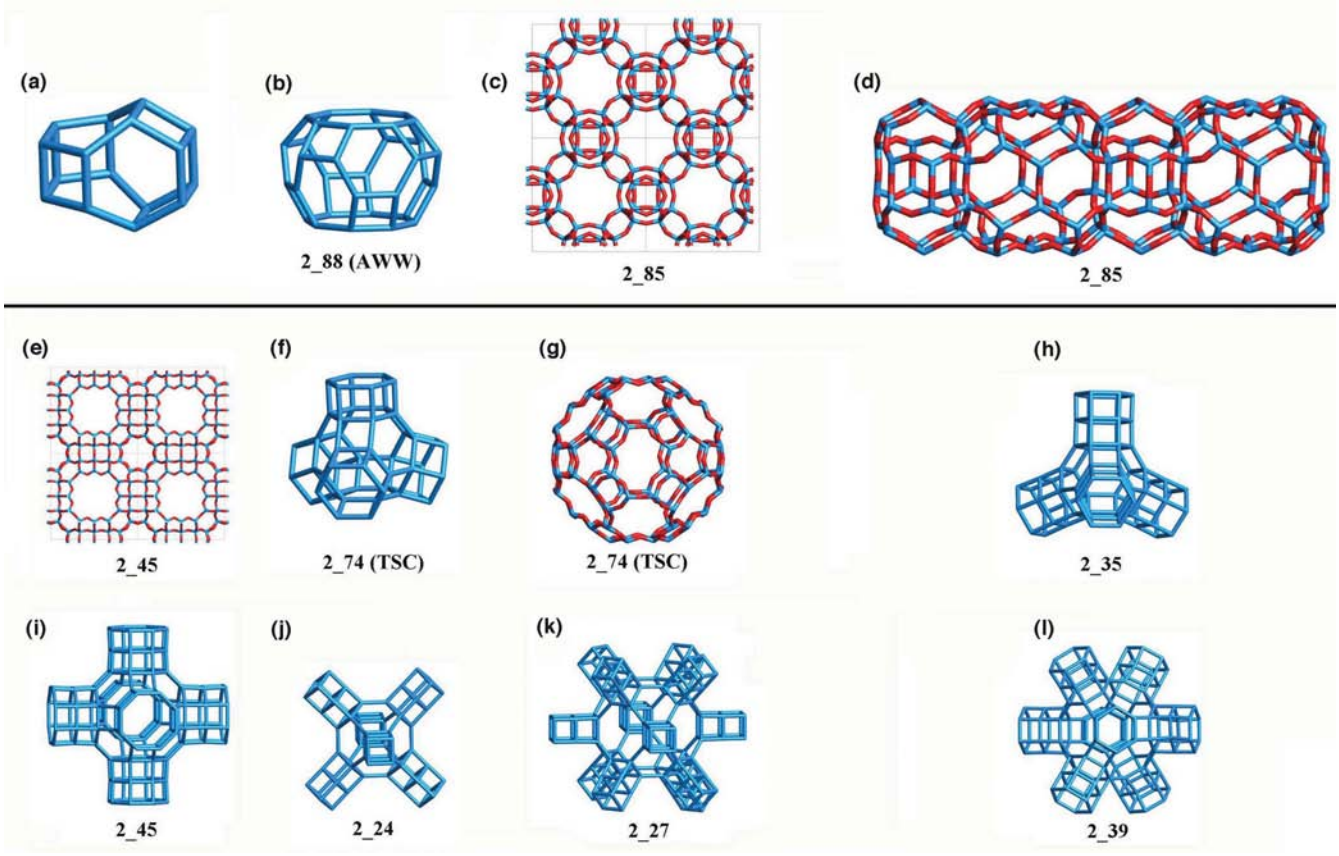

Figure 5
Molecular graphic illustrations of some structures from the AWW and supercage families.

and highly curved eight-rings. Structures 2_75, 2_6 or 2_76 are not expected to be chemically feasible.

3.11. Three- and four-ring family

These eight structures are grouped together because they contain both three- and four-membered rings, although in other ways they are fairly different. Seven structures are cubic and five have framework densities lower than 14 T per 1000 Å^3. Structure 2_99, the most feasible structure of this family with $\vartheta = 10.53$, can be described as a network of corner-sharing three- and four-rings, part of which is the unit shown in Fig. 8(*a*). Three types of cages are found, one of which is the [$3^8 8^6$] (truncated cube, Fig. 8*b*). The somewhat similar 2_62, which has $\vartheta = 10.97$, also exhibits the truncated cube cage. Structure 2_68 has a low framework density of 13.08 T per 1000 Å^3 and ϑ = 13.82. Structures 2_70 and 2_93 have similar framework densities to that of 2_68 (13.42 and 13.98, respectively) and ϑ = 14.33 and 28.25, making these three structures interesting candidates as zeotypes. Structure 2_93 contains [$3^4 6^4$] cages, *i.e.* truncated tetrahedra (Fig. 8*c*), which link through shared three-rings to form a body-centred cubic structure. Structures 2_18, 2_28 and 2_5 have much lower framework densities (10.06, 11.69 and 7.28, respectively) than conventional zeolites, and are thus much less feasible as zeotype materials.

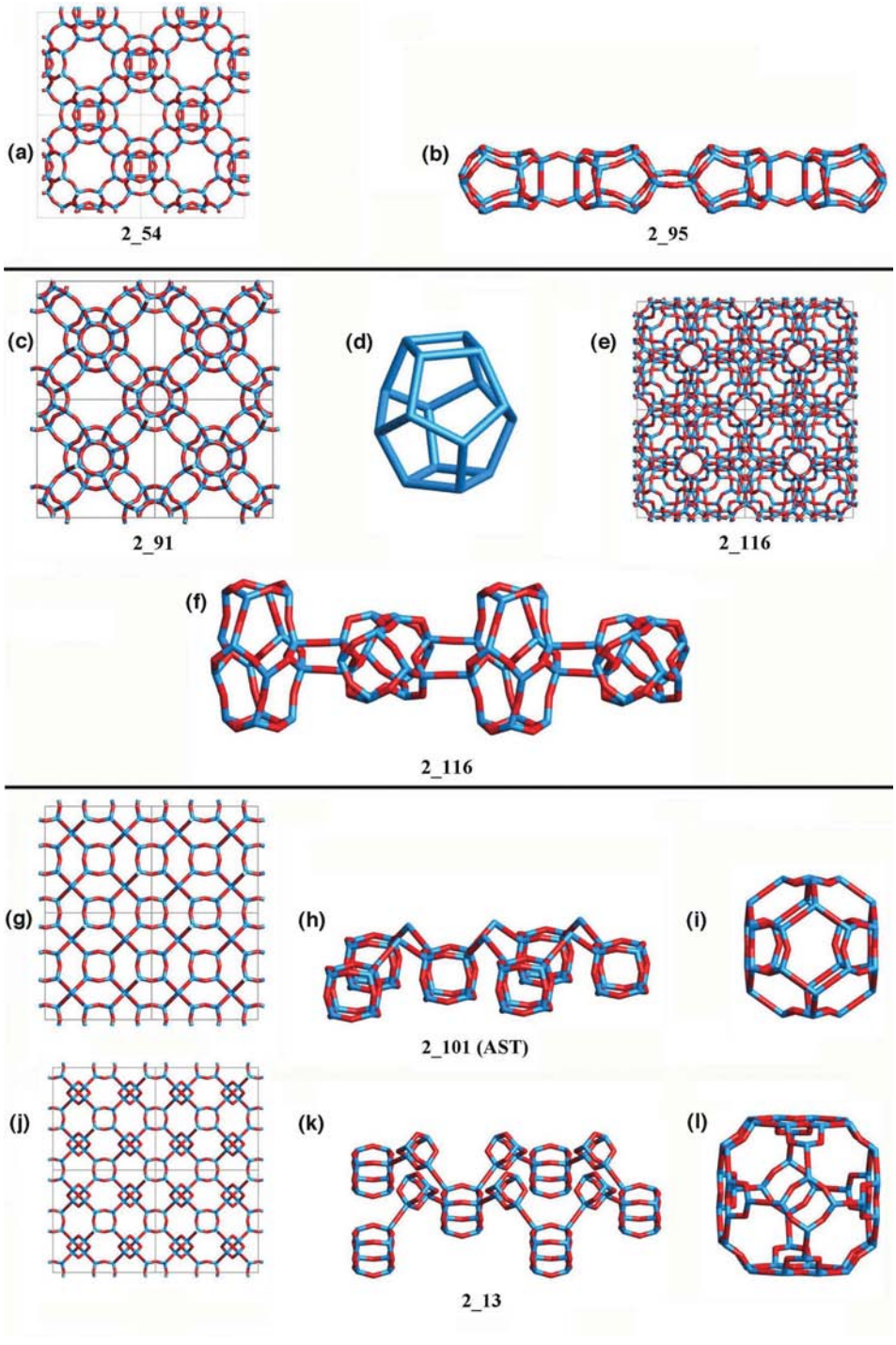

Figure 6
Molecular graphic illustrations of structures from the SAS, [$4^2 5^8$] and AST families.

3.12. [$3^2 4^3$] D3R family

The common feature is a trigonal prism (a [$3^2 4^3$] unit) and we have assigned nine structures to this family. As in the previous family, many are of interest due to their low density, with the presence of small polyhedra being compensated by large supercages. While we believe that none is feasible in a traditional zeolite or AlPO composition, they may be of interest in several areas of chemistry, for instance if it were possible to form the D3R unit as a precursor. All the structures are cubic and have at least $m\bar{3}m$ symmetry. Structure 2_43 (Figs. 8*d*–*f*) is the most feasible (ϑ = 11.62) and has D3R units attached to [$3^4 6^4$] truncated tetrahedra to form tetrahedral units (Fig. 8*e*). 'Truncated cube' cages are present, as are the large [$4^{24} 6^8 8^{18}$] cages shown in Fig. 8(*f*). In 2_64 the D3R are also attached to truncated cube cages, but the structure additionally

contains alpha and $[4^{24}6^{8}8^{18}]$ tschörtnerite (TSC) cages. Structure 2_23 has beta cages linked *via* D3R–four-ring–D3R bridging units and 2_26 also has the same unit of two D3R linked though a four-ring (as do 2_25 and 2_22), with alpha cages present. Structure 2_25 has a pore system connected through 12-ring apertures and contains, besides FAU supercages and LTA alpha cages, the large $[4^{24}8^{6}12^{8}]$ cages found in the RWY structure. Structure 2_41 is similar to 2_43, as the D3R form an alternating network with truncated tetrahedra (as in Fig. 8*e*). Structure 2_22 is also of very low density (F_D = 9.70 T per 1000 Å^3) and has the D3R connected so as to define D8R. Finally, 2_4 and 2_8 are among the least dense of all the binodal simple tile structures, with F_D of 5.39 and 6.48 T per 1000 Å^3, respectively. The basic building unit of 2_8 is two D3R stacked with an intervening D4R (Fig. 8*g*). In 2_4 the intermediate unit is absent and D3R units join directly through a shared four-ring. In both cases, very open cavity systems are constructed by connection of these units (Fig. 8*h*).

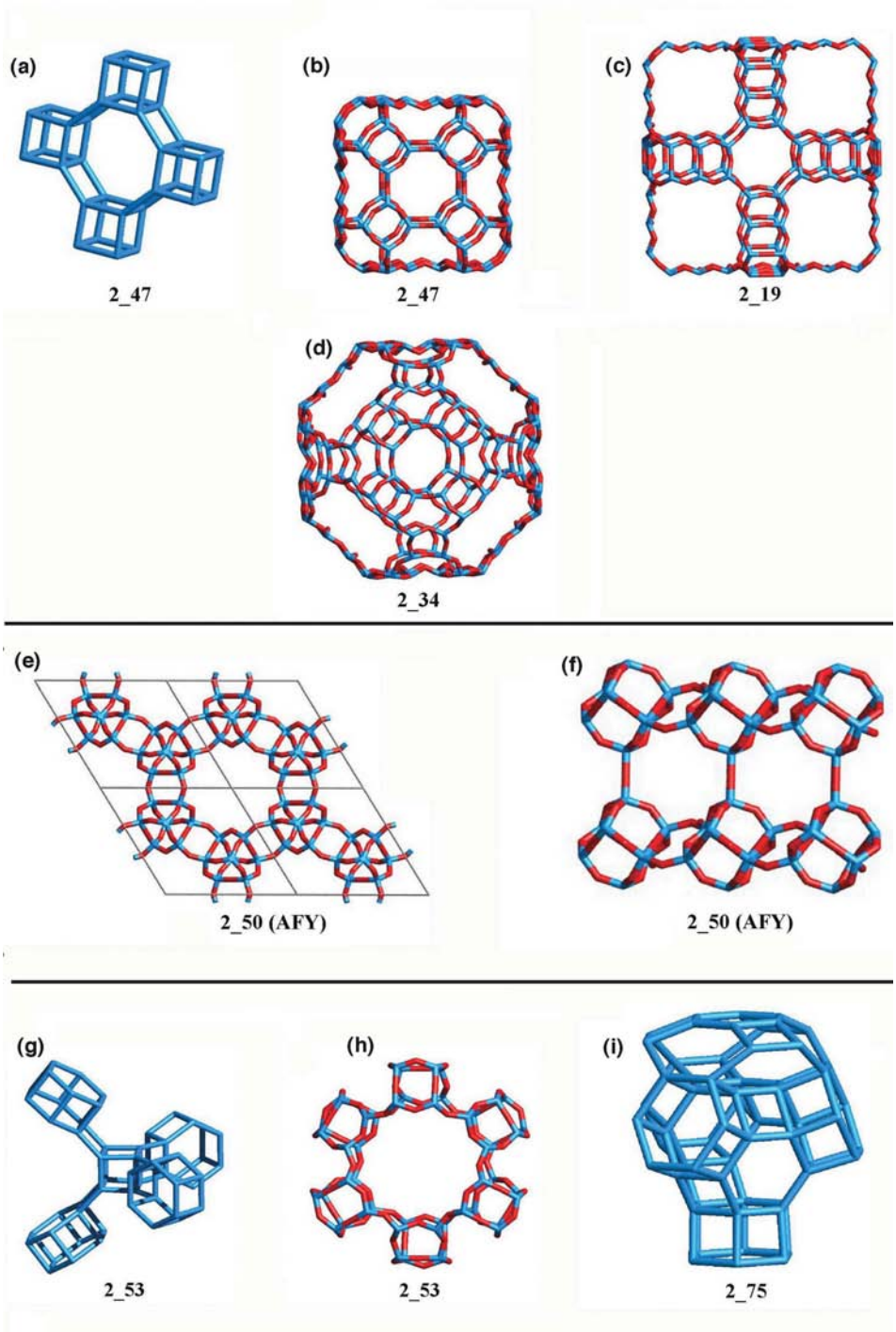

Figure 7
Molecular graphic illustrations of some structures from the D8R family, AFY structures and the D6R family.

3.13. Three-ring family

This family of eight structures is characterized by the presence of three-rings. Five structures contain pairs, or longer chains, of three-rings which share one T atom and therefore contain the spiro-5 unit (Baerlocher *et al.*, 2001). Two of the structures also contain four-rings. As expected, several of the structures are of low density, but none would be expected to be realisable as a conventional zeolite. In 2_71, the most feasible with ϑ = 17.07, three-rings themselves form rings of six (Fig. 8*i*), with the structure also containing elongated cages having eight-rings as their largest pore. The basic unit of 2_69 is a pair of edge-sharing three-rings (or bridged four-ring, Fig. 8*j*). These larger units then connect to define a hexagonal channel system. Structure 2_65 also contains loops of six three-rings, virtually identical in structure to those in 2_71. However, the structure is much more open (F_D = 12.28, compared with 17.38 for 2_71), containing a three-dimensional network of 10- and 12-ring pores. Structure 2_44 is another very open structure (F_D = 10.36), with a three-dimensional network of corner-sharing three-rings defining the small $[3^{4}6^{4}]$ cages shown in Fig. 8(*k*), as well as large cavities linked through 12-rings. Structure 2_12 has unusual chains built up from pairs of edge-sharing three-rings and has large cross-linked channels extending in two dimensions, delineated by puckered 14-membered rings (Fig. 8*l*). Structure 2_29 is an

unusually complex cubic structure, with three- and four-rings linked together (Fig. 8*m*): pairs of edge-sharing three-rings are formed (there are no spiro-5 units) and these pairs are further connected by distorted four-rings. Uniquely for this family, in 2_105 the three-rings do not directly link into chains or pairs through the sharing of *T* atoms, but rather connect through oxygen bridges to define five-rings. Finally, 2_9 has H-shaped building units in which four-rings share edges with pairs of three-rings (Fig. 8*n*).

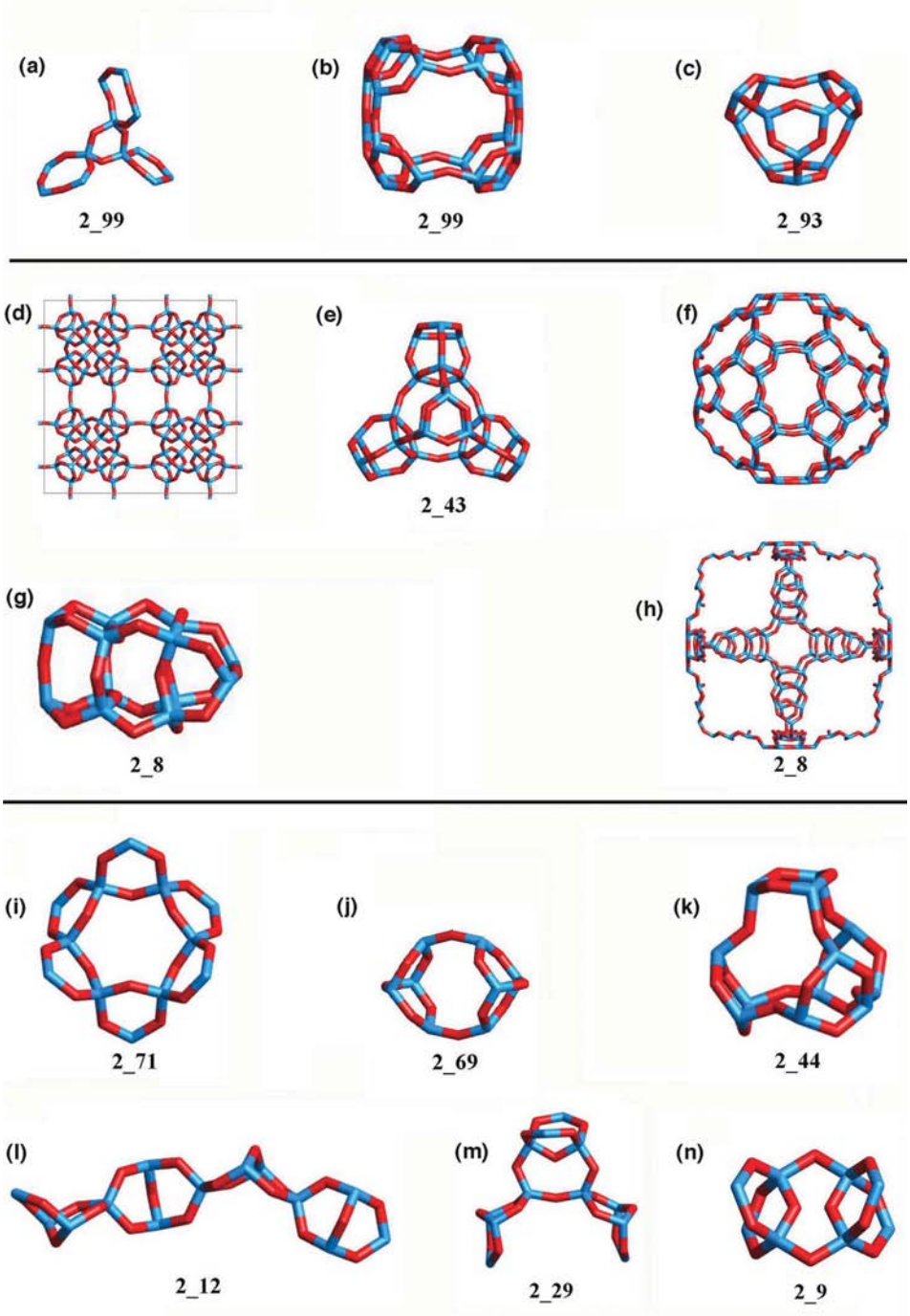

Figure 8
Molecular graphic illustrations of structures from the three- and four-ring family, the D3R family and the three-ring family.

3.14. [3^4] family

The common feature of this family is a [3^4] unit, sometimes known as the 'supertetrahedron' or 'tetrahedron of tetrahedra'. This unit is unknown in zeolitic oxide materials, but is present in some sulfides, including the zeotypic RWY structure and the compound $Na_2Si_2S_5$. Structure 2_16 (Figs. 9*a* and *b*), one of the few structures containing seven-rings, is characterized by its [$3^8 4^2 7^8 8^4$] cage (Fig. 9*b*). Each of the eight three-rings forms part of a [3^4] unit, shared with three other cages. This structure is the most feasible of this family, with ϑ = 36.19. Similarly, 2_14 has only one type of 'larger' cage, [$3^8 4^2 6^4 8^8$], and the whole structure can be thought of in terms of the sodalite framework, but with one third of the *T* sites replaced by [3^4] supertetrahedra. Structure 2_15 is also related to the sodalite structure, although now with half of the original *T* sites replaced by the [3^4] units, creating [$3^{12} 6^6 9^8$] cages. Structure 2_10 can be derived from the RHO zeolite structure by replacement of all *T* sites by [3^4] tetrahedra. As a result, it possesses very large cages linked *via* double 16-membered rings (Fig. 9*c*). Finally, structure 2_7, being the least dense of this family (F_D = 8.60), has [$3^4 6^4$] units ('truncated tetrahedra') linked *via* chains of four-rings and [3^4] units (Fig. 9*d*). This very open cubic structure has 16-MR pores in all three dimensions.

3.15. Orphan structures

We show three selected structures out of the 12 which cannot be categorized in our 'family' system.

Structure 2_96, a feasible zeolite structure (ϑ = 5.45), is unusual as it contains small [$4^5 5^2 6^2$] cage units (Fig. 9*e*) interconnected through shared four-rings to form a three-dimensional network (Fig. 9*f*), thereby defining the [$5^{12} 6^{20}$] cage which also appears in structure 2_97.

Structure 2_37 (Figs. 9*h–j*): the basic building unit is the D4R, which links *via* four-rings to create double 12-membered rings (Fig. 9*i*), which are in turn linked into

large [$4^{36}8^4 12^8$] supercages with tetrahedral symmetry, with four puckered 12-rings and four 12-rings which are almost planar (Fig. 9*j*). This cubic structure is quite open with F_D = 12.58 T per 1000 Å^3, but is of intermediate feasibility (ϑ = 18.50).

Structure 2_94 (Figs. 9*k* and *l*) contains [$3^4 6^4$] truncated tetrahedra, distorted sodalite cages, and larger cages with three- and six-rings (Fig. 9*l*). The ideal symmetry of the structure is $Fd\bar{3}m$. However, in silica form it appears highly strained in this symmetry, preferring to minimize in space group $C2$, giving rise to its somewhat distorted appearance.

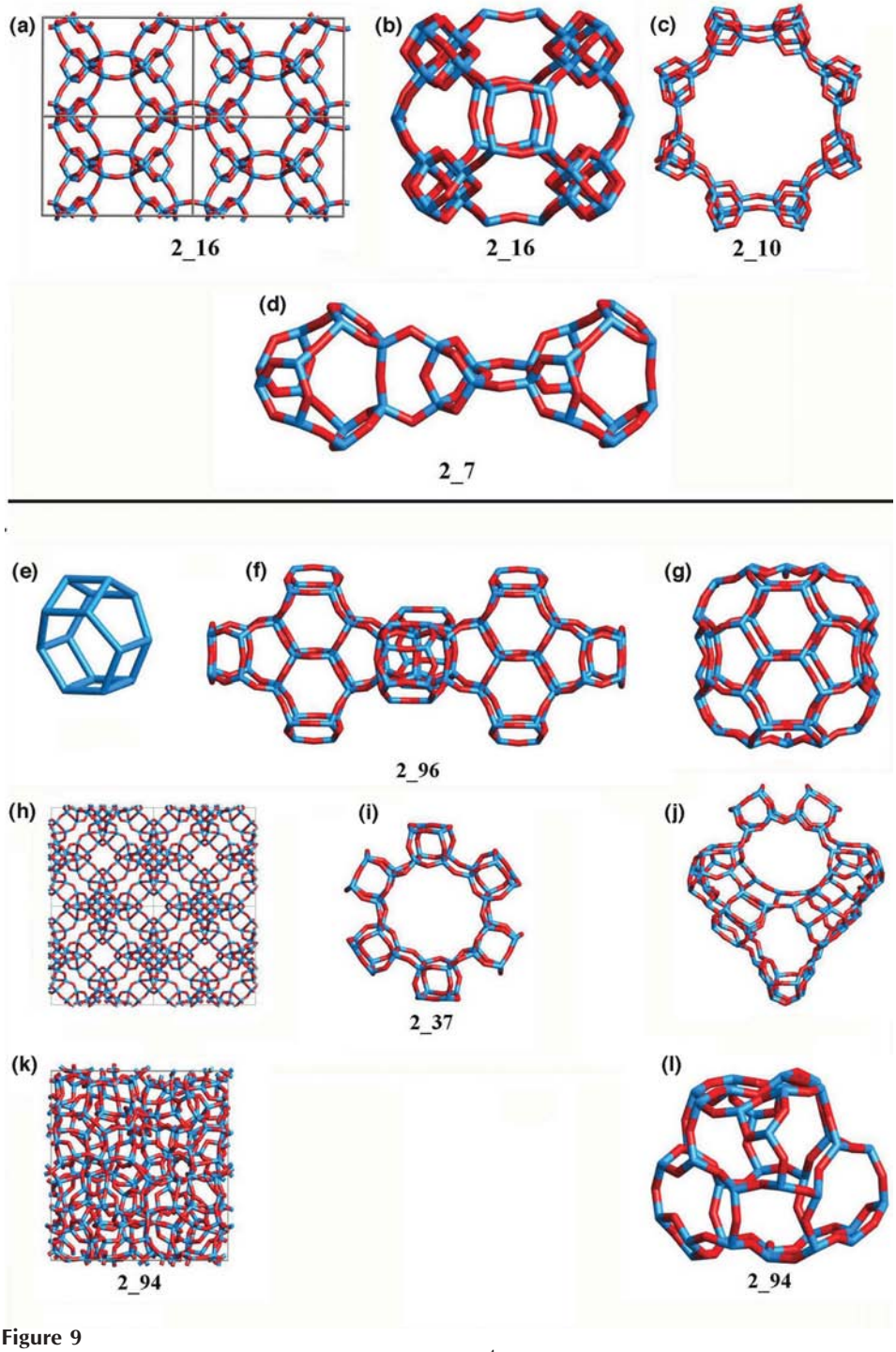

Figure 9
Molecular graphic illustrations of structures from the [3^4] family and of some of the orphan structures.

4. Conclusions

We have evaluated and characterized 109 hypothetical zeolite structures, of which 98 do not correspond to known zeotype frameworks. Among these are many promising candidates for zeolite synthesis. Some of the most feasible as conventional aluminosilicates or AlPOs are those in the ABC-6 family, composed principally of four- and six-rings, although from the point of view of porosity, the more likely structures will be at best small-pore zeolites, having no aperture larger than the eight-ring. Other promising candidates come from structures which similarly have features in common with known zeolites, such as those in the AWW and SAS families (Figs. 5 and 6), where cages stack through shared eight-rings. Again, four- and six-rings predominate, with the eight-ring being the limiting aperture in all cases, as it is for the more feasible structures in the [$4^2 5^6$] family. At the other end of the scale, many very open structures also exist. These illustrate well the principle (Brunner & Meier, 1989) that less dense structures require a greater proportion of small (three- or four-membered) rings. Here, we can extend this to state that larger cavities also require the presence of much smaller cages. Hence, we find large-pore structures containing [3^4] units (Fig. 9), double three-rings (Fig. 8) and three-rings, as well as pairs and chains of three- and four-rings. In terms of aluminosilicate and aluminophosphate zeolites, these structural units, particularly those containing three-rings, are by and large disfavoured due to the strain imposed on the TO_4 tetrahedra. In fact, it is apparent that feasibility decreases markedly as more three-rings are connected together with, for example, structures containing [3^4] units having higher values than those containing only spiro-5 units. The most viable

three-ring structures are those in which the three-rings are isolated from one another. The best example is 2_103 which contains the $[3^2 5^6]$ unit (Fig. 4*g*), reminiscent of the $[3^1 4^3 5^3]$ units in the MEI structure. Structure 2_103 is the most feasible large-pore zeolite among our 109 structures. Similarly, although four-rings are found in the most feasible structures, agglomerations of these units, obtained by stacking prismatic units such as D4R and D6R, result in decreasing likelihood (although individual D4R and D6R are tolerated, unlike D3R).

Having discounted many of the more open structures as potential zeolites on account of the presence of these small units, we do not exclude the possibility that these topologies could be possible in other chemical compositions where the local coordination environments are less constrained. Indeed, if we could construct units such as the D3R or the super-tetrahedron as precursor species, many open framework architectures could be synthesized.

We are grateful to the EPSRC (U.K.) and to the Leverhulme Trust for support, and to the Portuguese Foundation for Science and Technology (FCT) for the Ph.D. scholarship No. SFRH/BD/3024/2000 to F.A.A.P.

References

Akporiaye, D. E. & Price, G. D. (1989). *Zeolites*, **9**, 23–32.

Alberti, A. (1979). *Am. Mineral.* **64**, 1188–1198.

Baerlocher, C. & McCusker, L. B. (2004). http://www.iza-structure.org/databases.

Baerlocher, C., Meier, W. M. & Olson, D. H. (2001). *Atlas of Zeolite Structure Types* (updates at http://www.iza-structure.org/), 5th ed. London: Elsevier.

Barrer, R. M. & Villiger, H. (1969). *Z. Kristallogr.* **128**, 352–370.

Bialek, R. (1995). *KRIBER*, Version 1.1. Institut für Kristallographie und Petrographie, ETH, Zürich, Switzerland.

Boisen, M. B., Gibbs, G. V., O'Keeffe, M. & Bartelmehs, K. L. (1999). *Micropor. Mesopor. Mater.* **29**, 219–266.

Brunner, G. O. & Meier, W. M. (1989). *Nature*, **337**, 146–147.

Connolly, M. L. (1985). *J. Am. Chem. Soc.* **107**, 1118–1124.

Delgado Friedrichs, O. (2001). *Discret. Comput. Geom.* **26**, 549–571.

Delgado Friedrichs, O., Dress, A. W. M., Huson, D. H., Klinowski, J. & Mackay, A. L. (1999). *Nature*, **400**, 644–647.

Dress, A. W. M., Huson, D. H. & Molnár, E. (1993). *Acta Cryst.* A**49**, 806–817.

Foster, M. D., Bell, R. G. & Klinowski, J. (2001). *Stud. Surf. Sci. Catal.* **136**, 266.

Foster, M. D., Delgado Friedrichs, O., Bell, R. G., Almeida Paz, F. A. & Klinowski, J. (2003). *Angew. Chem. Int. Ed.* **42**, 3896–3899.

Foster, M. D., Friedrichs, O. D., Bell, R. G., Almeida Paz, F. A. & Klinowski, J. J. (2004). *Am. Chem. Soc.* **126**, 9769–9775.

Foster, M. D., Simperler, A., Bell, R. G., Delgado Friedrichs, O., Almeida Paz, F. A. & Klinowski, J. (2004). *Nature Mater.* **3**, 234–238.

Foster, M. D. & Treacy, M. M. J. (2004). *Hypothetical Zeolites: Enumeration Research*; http://www.hypotheticalzeolites.net/ 2004.

Henson, N. J., Cheetham, A. K. & Gale, J. D. (1994). *Chem. Mater.* **6**, 1647–1650.

Hu, Y. T., Navrotsky, A., Chen, C. Y. & Davis, M. E. (1995). *Chem. Mater.* **7**, 1816–1823.

Klinowski, J. (1998). *Curr. Opin. Solid State Mater. Sci.* **3**, 79–85.

Koningsveld, H. van (2004). *Schemes for Building Zeolite Structure Models*, in *Database of Zeolite Structures*; http://topaz.ethz.ch/IZA-SC/ModelBuilding.htm.

Liebau, F., Gies, H., Gunawardane, R. P. & Marler, B. (1986). *Zeolites*, **6**, 373–377.

Meier, W. M. (1986). *Zeolites and Zeolite-Like Materials.* 7th Int. Zeolite Conference, Tokyo, 17–22 August.

Meier, W. M. & Villiger, H. (1969). *Z. Kristallogr.* **128**, 352–370.

Mellot-Draznieks, C., Girard, S., Férey, G., Schön, J. C., Cancarevic, Z. & Jansen, M. (2002). *Chem. Eur. J.* **8**, 4103–4113.

Mellot-Draznieks, C., Newsam, J. M., Gorman, A. M., Freeman, C. M. & Férey, G. (2000). *Angew. Chem. Int. Ed.* **39**, 2270–2275.

Molecular Simulations Inc. (1999). *Cerius*^{2}, Version 4.0. Molecular Simulations Inc., San Diego, USA.

Moloy, E. C., Davila, L. P., Shackelford, J. F. & Navrotsky, A. (2002). *Micropor. Mesopor. Mater.* **54**, 1–13.

O'Keeffe, M. & Hyde, S. T. (1996*a*). *Z. Kristallogr.* **211**, 73–78.

O'Keeffe, M. & Hyde, B. G. (1996*b*). *Crystal Structures I: Patterns and Symmetry*. Mineralogical Association of America Monograph, Washington, DC.

Navrotsky, A., Petrovic, I., Hu, Y. T., Chen, C.-Y. & Davis, M. E. (1995). *Micropor. Mater.* **4**, 95–98.

Persistence of Vision Raytracer Pty. Ltd (2004). *POV-Ray*, Version 3.6. Persistence of Vision Raytracer Pty Ltd.

Petrovic, I., Navrotsky, A., Davis, M. E., Zones, S. I. (1993). *Chem. Mater.* **5**, 1805–1813.

Piccione, P. M., Laberty, C., Yang, S. Y., Camblor, M. A., Navrotsky, A. & Davis, M. E. (2000). *J. Phys. Chem. B*, **104**, 10001–10011.

Piccione, P. M., Woodfield, B. F., Boerio-Goates, J., Navrotsky, A. & Davis, M. E. (2001). *J. Phys. Chem. B*, **105**, 6025–6030.

Piccione, P. M., Yang, S. Y., Navrotsky, A. & Davis, M. E. (2002). *J. Phys. Chem. B*, **106**, 3629–3638.

Sastre, G. & Gale, J. D. (2001). *Micropor. Mesopor. Mater.* **43**, 27–40.

Sato, M. (1984). *Framework Topology and Systematic Derivation of Zeolite Structures*, edited by D. H. Olson and A. Bisio. In Proc. of the 6th Intl Zeolite Conference, Reno, USA, 10–15 July. Guildford: Butterworths.

Sato, M. J. (1987). *Phys. Chem.* **91**, 4675–4681.

Sherman, J. D. & Bennett, J. M. (1973). *Molecular Sieves*, edited by W. M. Meier and J. B. Uytterhoeven, Vol. 121, p. 52. Washington, DC: American Chemical Society.

Simperler, A., Foster, M. D., Bell, R. G. & Klinowski, J. (2004). *J. Phys. Chem. B*, **108**, 869–879.

Smith, J. V. (1988). *Chem. Rev.* **88**, 149–182.

Smith, J. V. (1993). *ACS Abstr.* **205**, 157-IEC.

SourceForge (2004). *GDIS*, Version 0.84. SourceForge.

Treacy, M. M. J., Randall, K. H., Rao, S., Perry, J. A. & Chadi, D. J. (1997). *Z. Kristallogr.* **212**, 768.

Wells, A. F. (1977). *Three-Dimensional Nets and Polyhedra*. New York: Wiley.

Wells, A. F. (1979). *Further Studies of Three-Dimensional Nets*, American Crystallographic Association Monograph No. 8, Vol. 9. Pittsburgh, PA: Polycrystal Book Service.

Wells, A. F. (1984). *Structural Inorganic Chemistry*, 5th ed. Oxford University Press.